FINAL REPORT

Contract NAS8-39950

"Surface Conversion Techniques for Low Energy Neutral Atom Imagers"

Research Funded by
"Techniques and Technologies for Magnetospheric Imaging"
MSFC NRA 8-8

Report Date: 14 March 1995

Prepared By: J.M. Quinn
Lockheed R&DD
415-424-3289

INTRODUCTION

This investigation has focused on development of key technology elements for low energy neutral atom imaging. More specifically, we have investigated the conversion of low energy neutral atoms to negatively charged ions upon reflection from specially prepared surfaces. This "surface conversion" technique appears to offer a unique capability of detecting, and thus imaging, neutral atoms at energies of 0.01 - 1 keV with high enough efficiencies to make practical its application to low energy neutral atom imaging in space. Such imaging offers the opportunity to obtain the first instantaneous global maps of macroscopic plasma features and their temporal variation.

Through previous in situ plasma measurements, we have a statistical picture of large scale morphology and local measurements of dynamic processes. However, with in situ techniques it is impossible to characterize or understand many of the global plasma transport and energization processes. A series of global plasma images would greatly advance our understanding of these processes and would provide the context for interpreting previous and future in situ measurements.

Fast neutral atoms, created from ions that are neutralized in collisions with exospheric neutrals, offer the means for remotely imaging plasma populations. Energy and mass analysis of these neutrals provides critical information about the source plasma distribution.

The flux of neutral atoms available for imaging depends upon a convolution of the ambient plasma distribution with the charge exchange cross section for the background neutral population. Some of the highest signals are at relatively low energies (well below 1 keV). This energy range also includes some of the most important plasma populations to be imaged, for example the base of the cleft ion fountain.

Neutral atom fluxes are typically many orders of magnitude lower than that of charged particles, thus a high efficiency detection technique is required. Conventional methods, such as electron beam or field ionization, do not have adequate efficiency for application to magnetospheric imaging. Carbon foil techniques are well established for space plasma instrumentation at energies above 1 keV. However, below 1 keV, the efficiency of carbon foil ionization falls off very rapidly. Integral techniques, using direct detection combined with UV rejection, offer reasonable efficiency but cannot identify the neutral atom's mass or energy, and thus cannot address many of the key deconvolution and science issues.

In order to determine mass and energy of the imaged neutrals the incident atoms must be ionized for analysis. The use of surface conversion techniques to ionize incident neutrals offers the potential to fill the important energy gap below approximately 1 keV.

Figure 1 illustrates a neutral imaging instrument concept that uses the surface conversion technique. Neutral and charged particles enter the instrument through aperture B1, and are collimated in energy and angle. Ions and electrons are deflected by an electrostatic deflector and broom magnet, allowing the remaining neutrals to impinge upon the conversion surface (C). The neutrals that undergo charge exchange at the surface (to become negative ions) are accelerated away and collected by a wide aperture, low aberration, lens (L), which focuses the ions in the plane of slit S2. Transmitted ions are imaged by a spherical analyzer (EA) and further accelerated onto a carbon foil entrance to a time-of-flight section.

Surface conversion of neutral atoms is well established in laboratory experiments where it was developed in conjunction with fusion research. However, its application to spaceflight

instrumentation awaits resolution of important technological challenges. In particular, we need to: demonstrate the capability to manufacture conversion surfaces suitable for spaceflight, determine the efficiency of these surfaces, and investigate issues of surface stability. This investigation addresses these questions.

PROGRESS

This investigation has three key "target" areas of research. The first is to investigate neutral-to-ion conversion efficiency for a variety of surfaces and coatings as a function of incident energy and species. The second target area is to characterize yield dependencies on impact and scattering angle. The third target is to study long term stability of the surfaces and techniques for avoiding or minimizing regeneration requirements.

Many of the results described below have been submitted for publication by Wurz et al. (1994) and will be presented in Aellig et al. (1995) and Wurz et al. (1995).

The basic approach of the conversion technique is to use a conversion surface with a low work function to convert atoms with a high electron affinity to negative ions. H and O atoms, with electron affinities of 0.75 eV and 1.46 eV respectively, are good candidates for charge exchange, and are also ideal from the standpoint of being major species in the magnetosphere. Various surfaces have been either shown in the laboratory, or predicted theoretically, to be good converter candidates.

The laboratory measurements under this project are guided by theoretical analyses and computer modeling of surface interactions at the University of Bern, building upon previous work associated with fusion research. In particular, the "TRIM" and "MARLOWE" codes have been used at Bern to calculate conversion yields from various surfaces. Figures 2 and 3 illustrate the calculated conversion efficiency for neutral H from a cesiated W surface as a function of energy and impact angle. These analyses predict a relatively high efficiency at energies below 1 keV, and indicate that a fairly shallow impact angle onto the converter surface will be required in a practical space instrument.

As they scatter from the conversion surface, the newly created ions leave with an angular spread about the nominal specular reflection angle. This angular breadth is an important factor in the design of the collection lens and the energy/mass analyzing optics. Figure 4 shows the results of a MARLOWE simulation of the angular spread of H atoms when scattered from two promising conversion surfaces, tungsten with a cesium layer, and silver with a barium layer The figure illustrates the dependence of angular spread on energy for incident angles from 65^{o} - 80^{o}.

Figure 5 shows the total conversion efficiency results of the MARLOWE simulation over the same range of energies and incident angles as in Figure 4. These simulations support the promise of the technique for application to a neutral imaging instrument.

In order to establish the viability of the surface conversion technique for spaceflight instrumentation, it is essential to measure the performance of candidate surfaces in the laboratory, and to establish the rate at which surface deterioration degrades the efficiency. A number of promising candidates have been identified in the simulation studies.

Several test surfaces were prepared by the participating institutions for laboratory investigation. The manufacture of these surfaces requires special attention to both the underlying substrate and the application of the active surface. Although overall surface "flatness" (variations on a large scale across the surface) is not highly important to conversion efficiency, a high degree of "smoothness" (on an atomic scale) is required so that the scattering atoms interact with a locally smooth surface. One of the most readily

available materials for a smooth substrate is silicon. Si substrates with very high smoothness are available at relatively low cost due to the large investment of the microelectronics industry in their production. After exploring several alternatives, we obtained a total of 90 Si substrates from two different vendors.

Figure 6 is a photograph of one of the Si substrates used at Lockheed for deposition of candidate conversion surfaces. The substrate is mounted in a test holder made at GSFC. The substrates are 0.75" square and 0.030" thick. The manufacturing process begins with a 6" silicon wafer, which is polished and cut into wafers. The polished surface is aligned to within 1 degree of the crystal plane. The surface smoothness is between 3 and 6 atomic layers. The measured RMS smoothness obtained from this process is typically sub-angstrom.

Gold and tungsten surfaces were applied to several Si substrates from each of the two vendors in a various processes for intercomparison. Tungsten sputtered surfaces, 100 Angstroms thick, were applied in the Lockheed Multilayer Deposition Facility. Gold and tungsten sputtered surfaces were also prepared at an outside supplier. Samples of all three surface types from each of the two substrate lots were provided to the University of Bern for evaluation in the ion bean test facility.

Figure 7 schematically illustrates the University of Bern test setup for neutral surface conversion. A positive ion beam is used instead of a neutral beam because of the advantages in ion beam control and characterization. As the positive ions approach the surface they are neutralized, so their interaction during scattering is the same as for neutrals. The surface under test is prepared by heating, to 1400 K, and then application of the monolayer or partial monolayer (e.g. of Cs). Then the surface is rotated into position for the beam. Ionization efficiency measurements are made by first measuring the total flux of particles scattered from the surface (ions and neutrals). Then the retarding potential analyzer (RPA) is set to reflect ions and only measure the neutrals. Taking into account the different detection efficiencies of ions and neutrals, the flux of negative ions is then calculated. The RPA is also used to verify that the reflected ions are still molecular hydrogen and to suppress secondary electrons.

The ion source delivers energies from 100 - 3,000 eV, analyzed to about 1%. The angular distribution of the scattered ion distribution is obtained from the two dimensional imaging detector, which can be rotated through approximately 100^{o} into different positions. The workfunction of the surface under test is measured in situ via photoelectric effect. Operating pressure of the U. Bern chamber is approximately $1x10^{7}$ Torr.

Results of tests in the Bern chamber on a cesiated tungsten surface are shown in Figure 8. The solid curve (left axis) shows ionization efficiency for 225 eV H_2 as a function of time after surface reconditioning. The dashed curve (right axis) shows the surface work function. Figure 8 illustrates two very important results for the application of surface ionization to spaceflight instrumentation.

One important result shown in Figure 8 is laboratory confirmation of high conversion efficiency for a conversion surface that could be practically flown in space. The use of in-flight surface reconditioning with a Cs dispenser was anticipated in the imaging instrument concept illustrated in Figure 1. The measured efficiencies shown in Figure 8, remaining above 1% even after a full day's degradation, are well within the range needed for application to spaceflight imaging.

The second result shown in Figure 8, perhaps the most important, is the temporal profile of surface degradation after reconditioning. The figure illustrates close tracking between the increasing surface work function and the decreasing conversion efficiency as the freshly regenerated surface is exposed to the residual gas in the vacuum chamber. One expects that when the gas load onto the surface is on the order of 1 monolayer, the performance of the conversion surface will show significant degradation. Since pressure in the test chamber is significantly higher than would be encountered in a well vented space instrument, we would expect the one day degradation rate seen in this test to translate into 10 or more days operation on orbit between reconditionings.

Based upon these promising results a number of follow-up measurements are underway at the University of Bern. GSFC has recently brought their test chamber on line and is beginning to make independent measurements of conversion efficiencies with different surfaces. At Lockheed we are exploring the fabrication of alloy surfaces for comparison with the results that have been obtained with Cs and Ba monolayers on W, Au, and Ag.

SUMMARY

An instrument concept for neutral imaging in the earth's magnetosphere has been developed for remote sensing of low energy plasma populations. Theoretical investigations and computer simulations suggest several potential materials which could provide efficient conversion surfaces to ionize neutral atoms for detection in such an instrument. Test samples of several of these candidate surfaces have been manufactured using a variety of techniques. Laboratory measurements confirm that the predicted conversion efficiencies are achievable, and demonstrate that the surface degradation rate is within acceptable limits for a practical space instrument.

The use of surface conversion as part of a practical spaceflight neutral particle imager appears to be feasible. This technique will provide high efficiency measurement capabilities at energies that cannot be adequately covered using other techniques.

FIGURE CAPTIONS

1 Schematic cross section of low energy neutral particle instrument. Key components are labeled: entrance collimation with elevation angle acceptance slits B1 and S1; ion and electron deflectors I-DEF and E-DEF; conversion surface C; cesium dispenser D; secondary electron guiding magnets M1 and M2; extraction lens L; energy limiting slit S2; spherical analyzer EA; and time-of-flight mass analyzer MA.

2 Calculated conversion efficiency for H at a 65 degree impact angle to a W(110) surface covered with partial monolayer or thick layer of cesium.

3 Conversion efficiency as a function of impact angle for H reflected from a W(110) surface covered with 0.6 monolayer of Cs.

4 FWHM angular spread for H atoms reflected from Cs/W(110) with one monolayer of Cs, and Ba/Ag(111) with two monolayers of Ba. Results are from a MARLOWE computer simulation. The individual curves are calculations for 65^{o}(solid line), 70^{o} (dashed), 75^{o} (pointed) and 80^{o} (dashed-pointed).

5 MARLOWE simulation results for total conversion efficiencies versus kinetic energy for H atoms reflected from Cs/W(110) and Ba/Ag(111) surfaces. Individual curves are for same angles as Figure 4.

6 Photograph of Si substrate upon which various conversion surfaces are deposited. Surface dimensions are 0.75" square.

7 Schematic layout of University of Bern neutral surface conversion test setup.

8 Measured ionization efficiency of 225 eV H_2 impinging at 80 degrees on a Cs/W(110) surface with approximately 1 monolayer Cs (solid line). Work function, measured with the photoelectric effect (dashed line) is also shown (right axis). The surface degradation with time is due to the moderate pressure in the vacuum chamber.

ILENA Instrument Concept

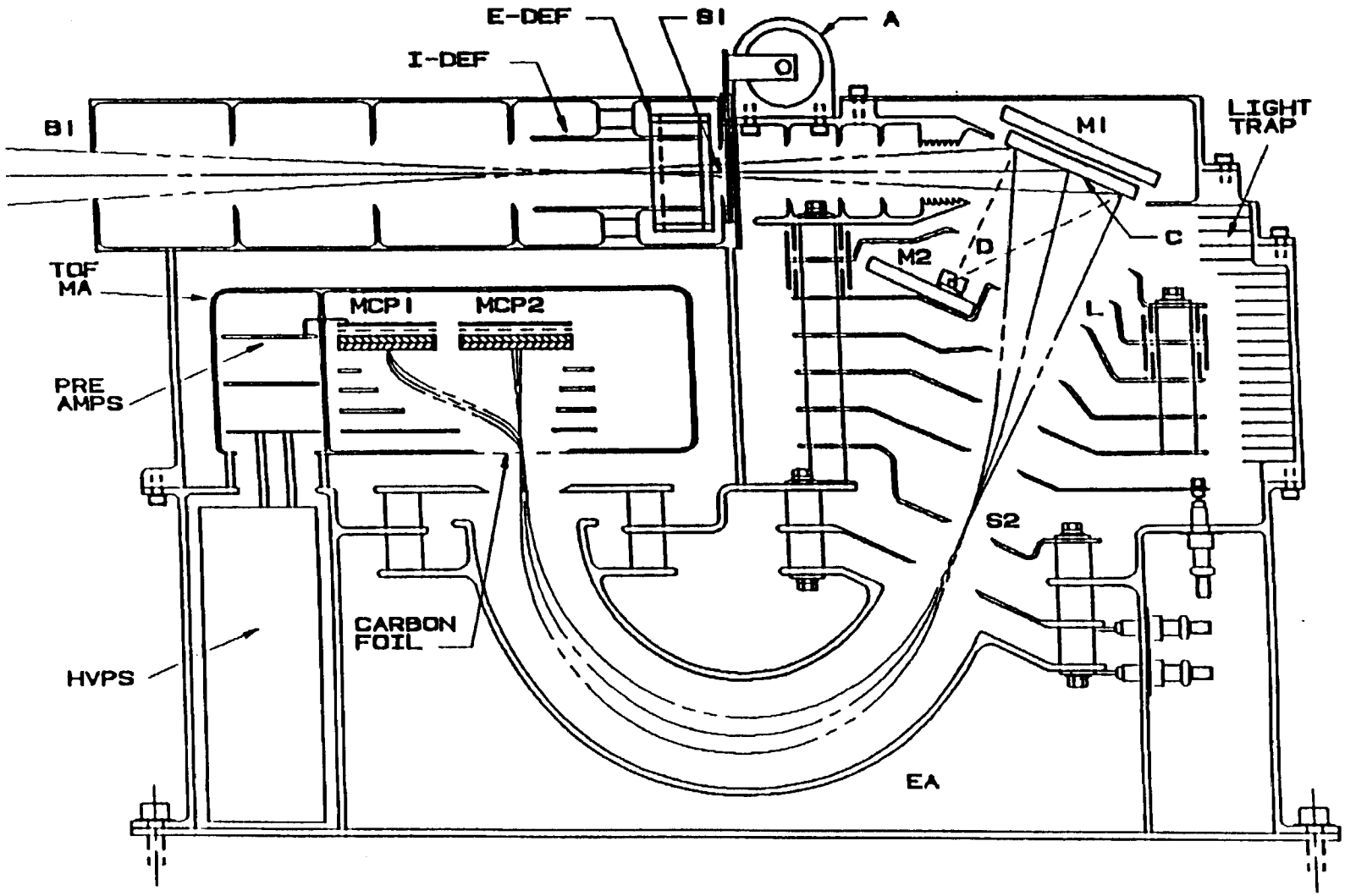

Figure 1

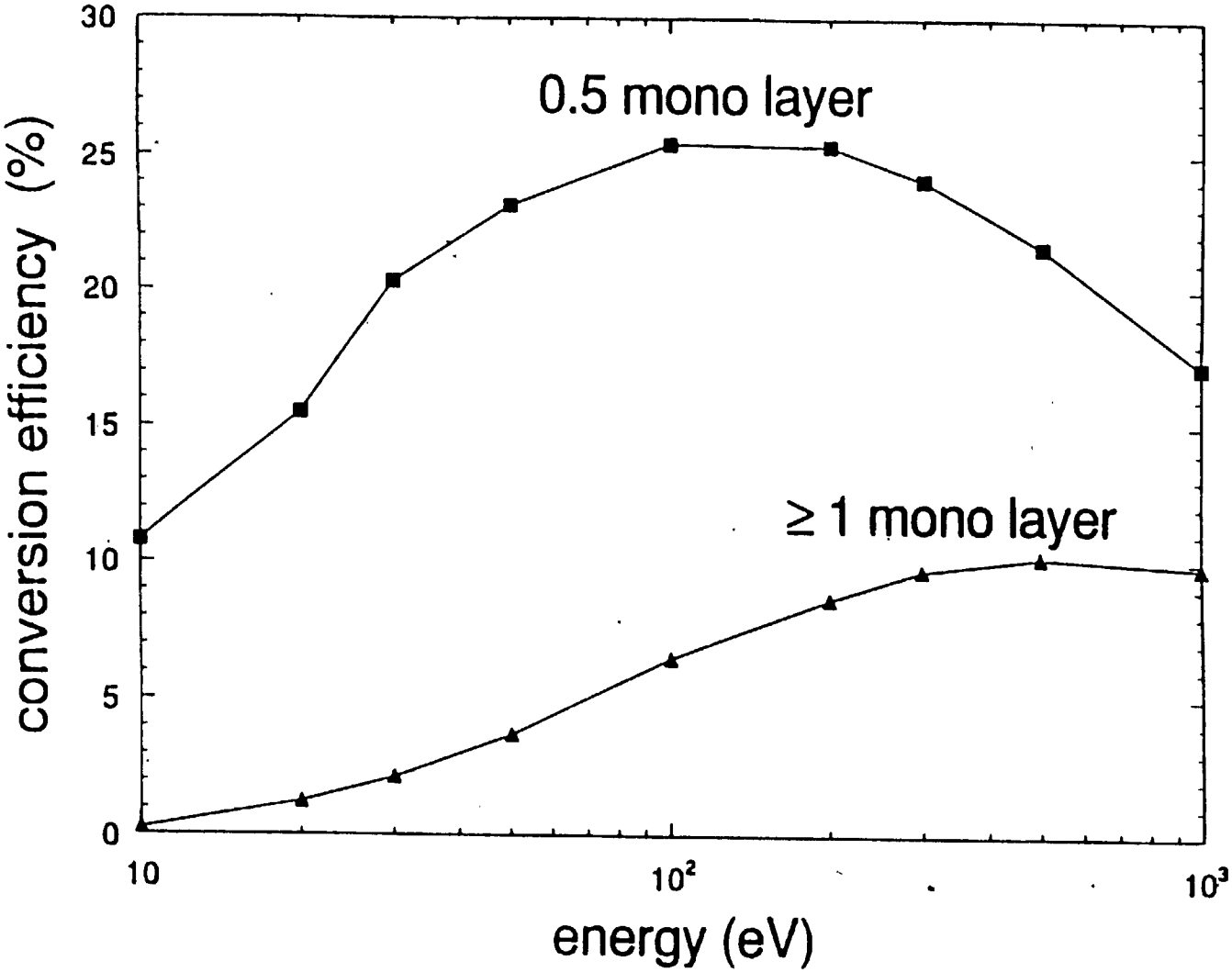
30
25
20
15
10
5
0
conversion efficiency (%)
0.5 mono layer
≥ 1 mono layer
10
10²
10³
energy (eV)

Figure 2

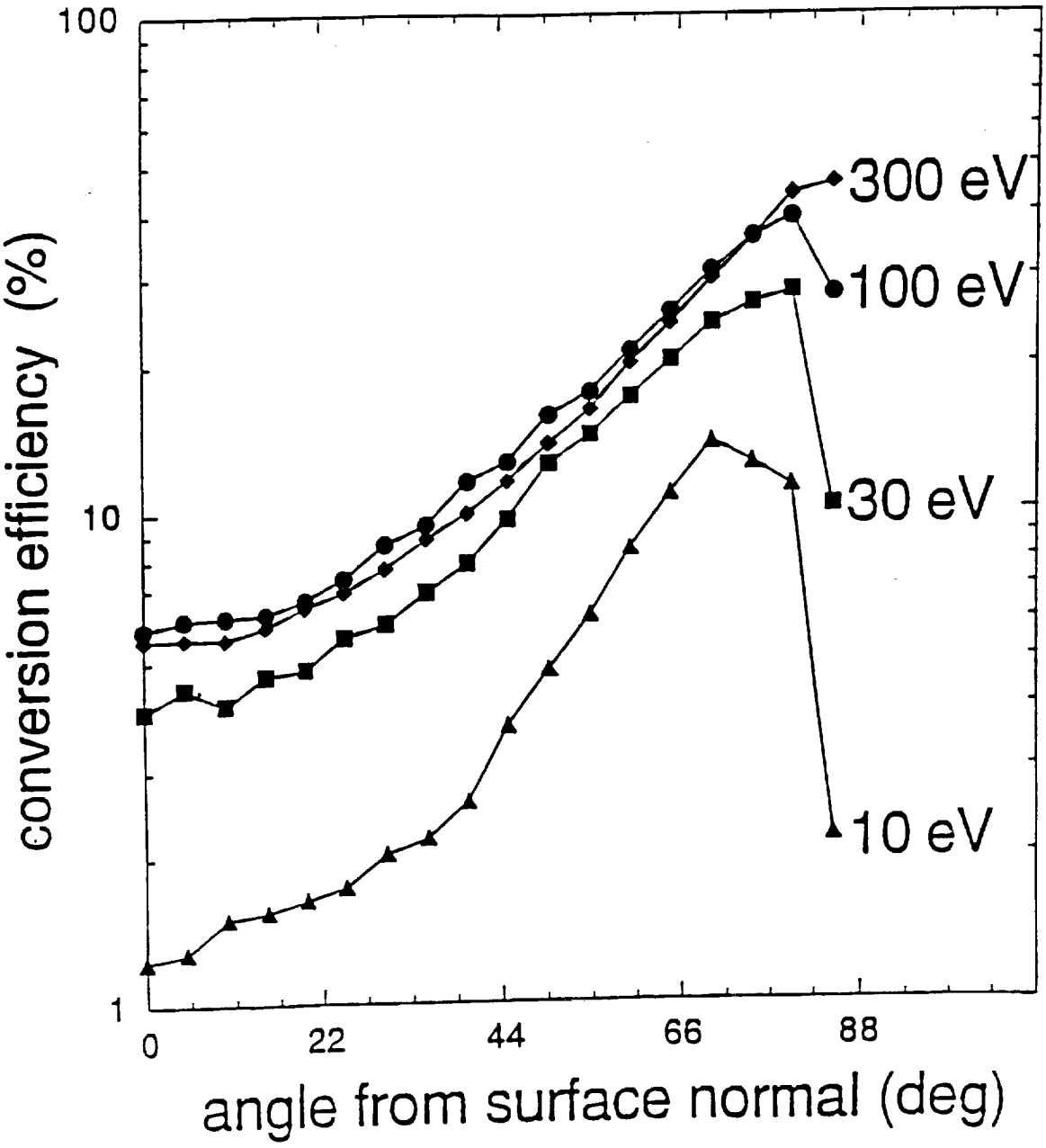
100
10
1
conversion efficiency (%)
0
22
44
66
88
angle from surface normal (deg)
300 eV
100 eV
30 eV
10 eV

Figure 3

Cs / W (110)

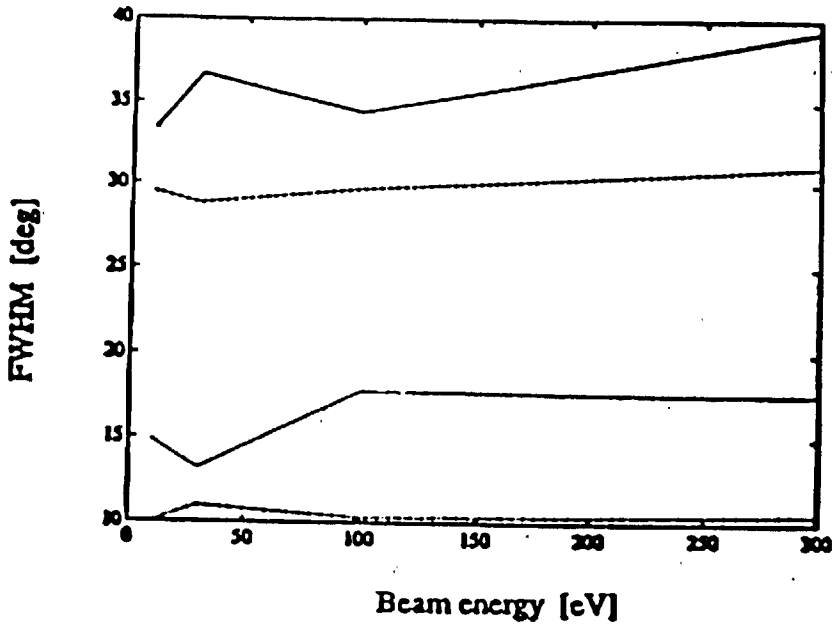

Ba / Ag (111)

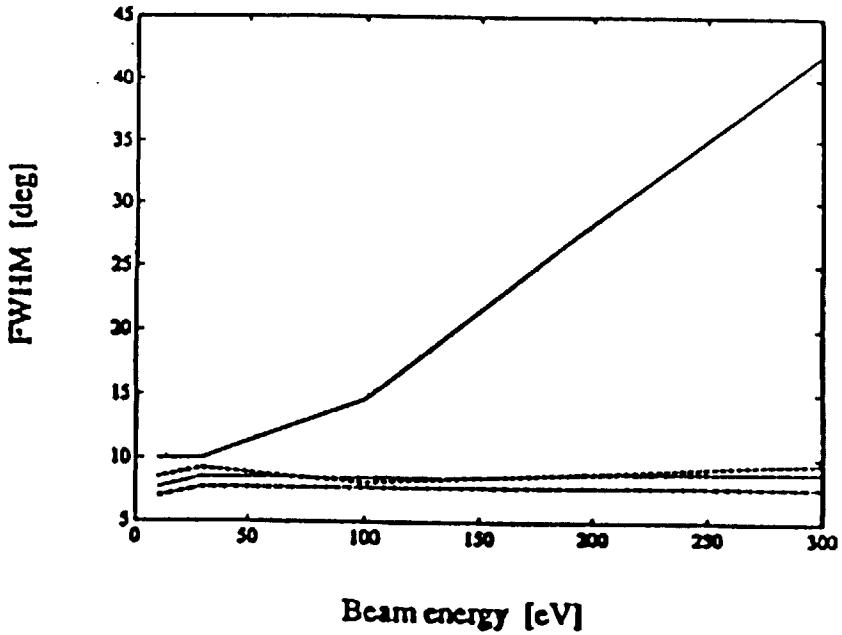

Figure 4

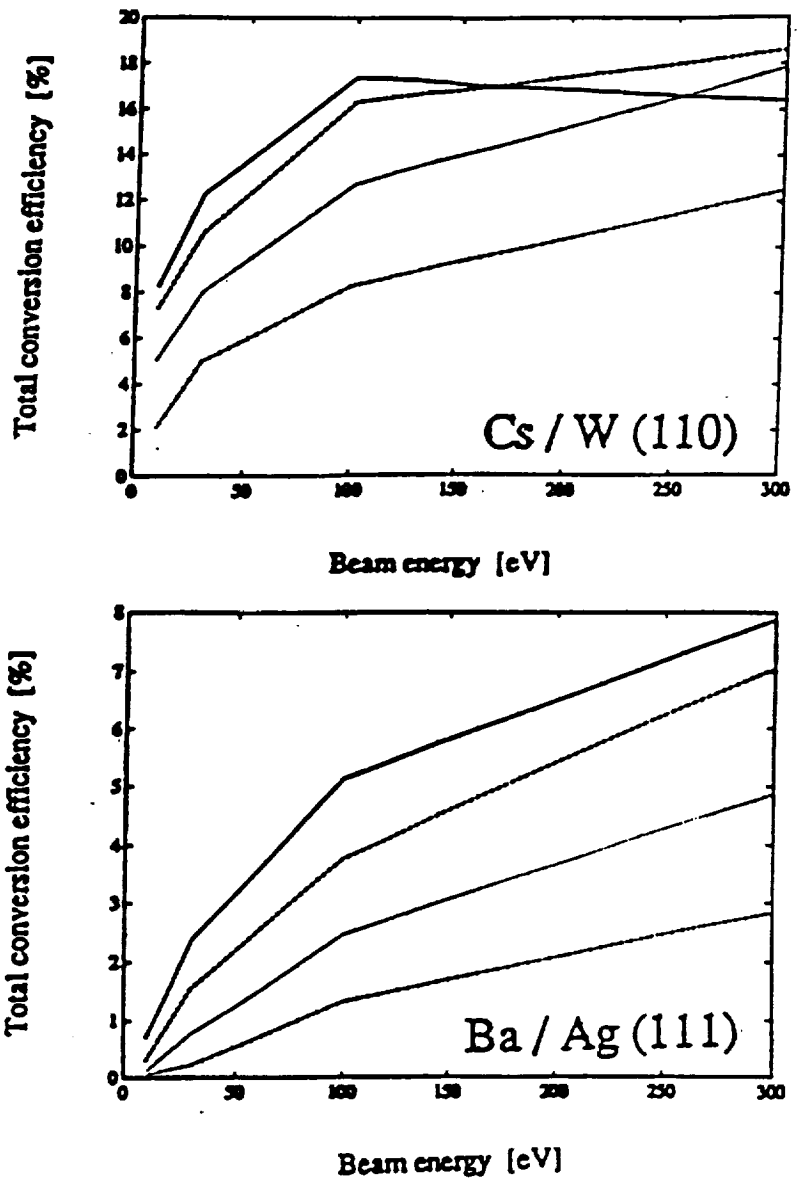
Total conversion efficiency [%]
Cs / W (110)
Beam energy [eV]
Total conversion efficiency [%]
Ba / Ag (111)
Beam energy [eV]

Figure 5

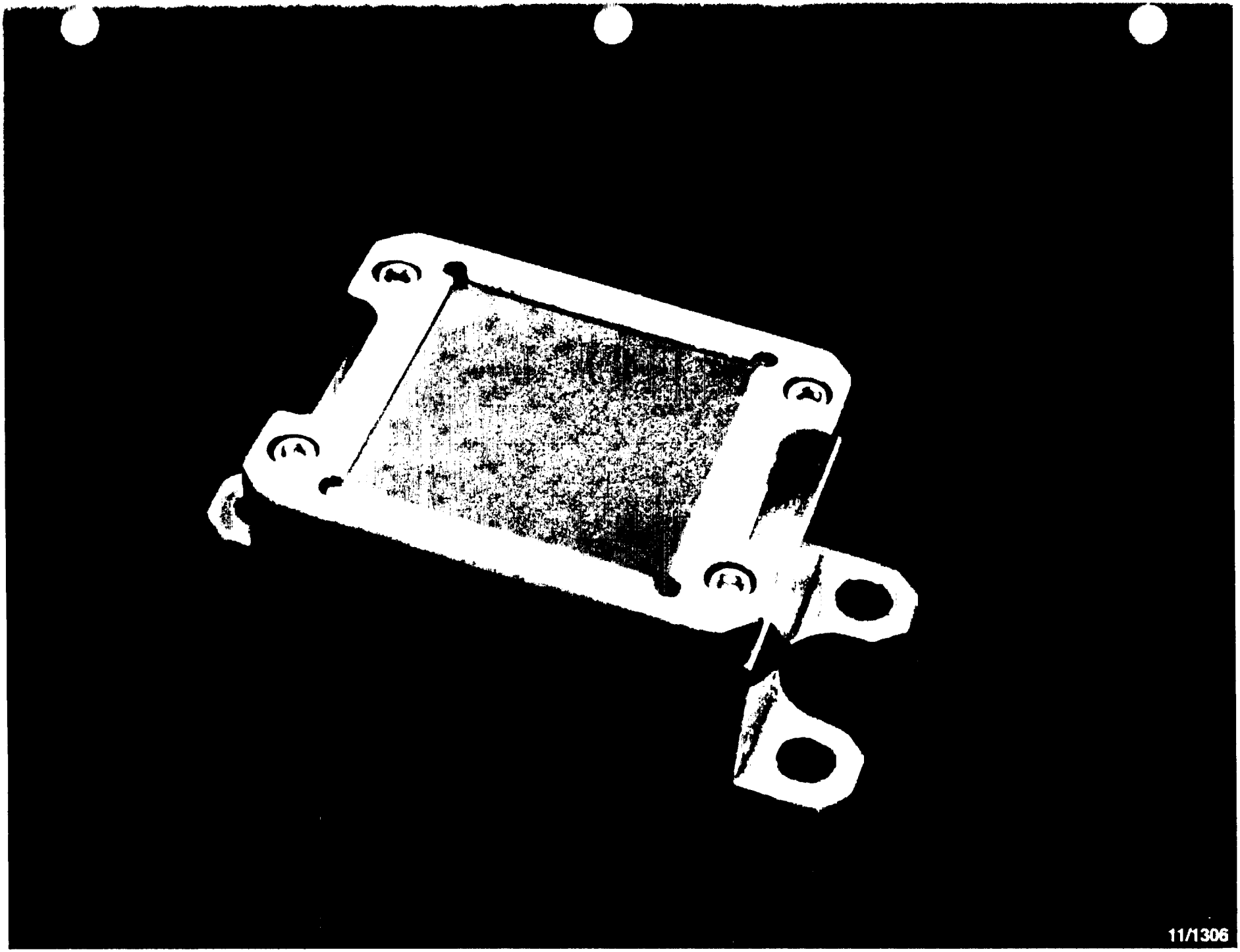
11/1306

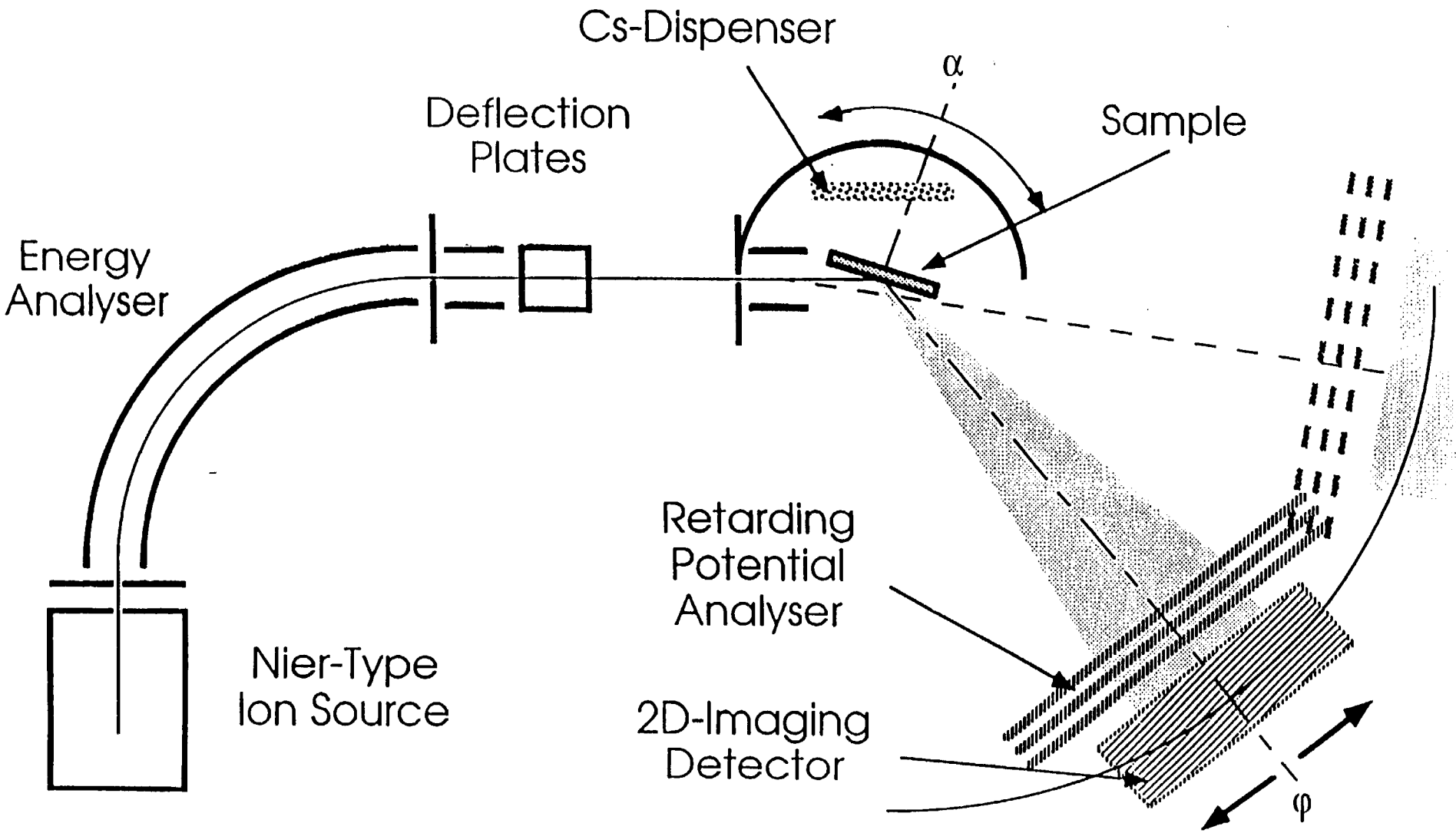
Cs-Dispenser
α
Deflection
Plates
Sample
Energy
Analyser
Retarding
Potential
Analyser
Nier-Type
Ion Source
2D-Imaging
Detector
φ

Figure 7

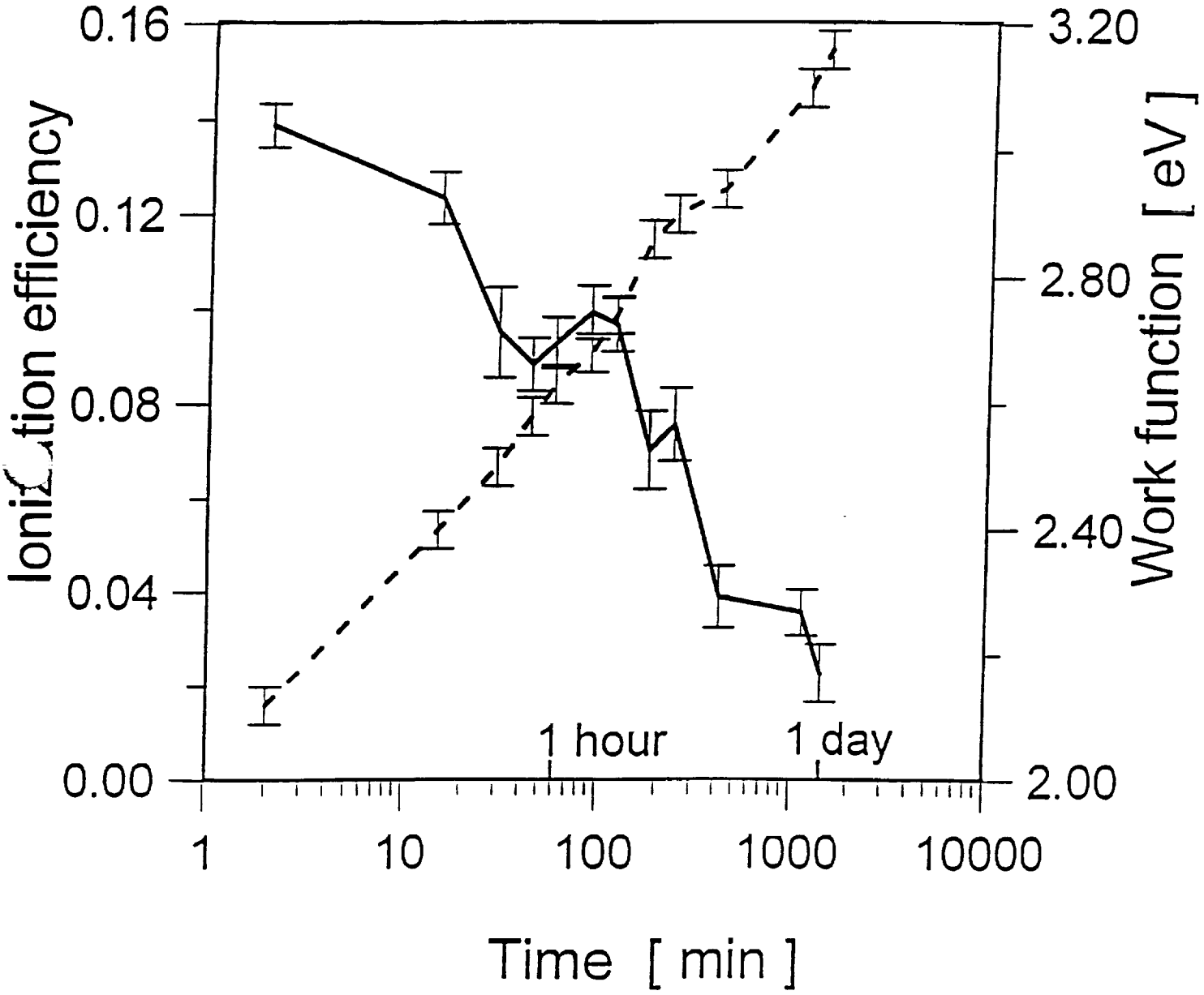
0.16
0.12
0.08
0.04
0.00
Ioniz tion efficiency
3.20
2.80
2.40
2.00
Work function [eV]
1 hour
1 day
1
10
100
1000
10000
Time [min]

Figure 8

PUBLICATIONS

Aellig, M.R., P. Wurz, P. Bochsler, A.G. Ghielmetti, J. Quinn, E.G. Shelley, S. Fuselier, F. Herrero, and M.F. Smith, Surface Ionization in Space Instrumentation, *Chapman Conference on Measurement Techniques for Space Plasma*, April 3-7, 1995.

Wurz, P, M.R. Aellig, P. Bochsler, A.G. Ghielmetti, E.G. Shelley, S. Fuselier, F. Herrero, M.F. Smith, and T. Stephen, Neutral Atom Imaging Mass Spectrograph, submitted to *Optical Engineering*, 1994.

Wurz, P., M.R. Aellig, P. Bochsler, F. Herrero, M.F. Smith, A.G. Ghielmetti, J. Quinn, E.G. Shelley, and S. Fuselier, Imager for Low Energy Neutral Atoms, *Chapman Conference on Measurement Techniques for Space Plasma*, April 3-7, 1995.

SURFACE IONIZATION IN SPACE INSTRUMENTATION

M. Aellig, P. Wurz, P. Bochsler (Physikalisches Institut, University of Bern)
A. Ghielmetti, J. Quinn, E. Shelley, S. Fuselier (Lockheed Palo Alto Research Laboratory)
F. Herrero, M. Smith (NASA GSFC)

Conversion of low energy atoms into negative ions with low work function surfaces is used routinely in fusion plasma research. The adaptation of this technique for use in space research makes the detection of low energy neutral particles possible even if fluxes are as low as in the interstellar neutral gas.

First measurements have shown that under vacuum conditions inferior to conditions encountered on spacecrafts, the cesiated tungsten surface stayed operational during one day. Ionization yields for molecular hydrogen of up to 15% have been observed. In addition to the high efficiency and ease of operation, no continuous power supply is required for this ionization method. A description of the apparatus as well as first results will be presented.

1. Chapman Conference on Measurement Techniques for Space Plasmas; April 3-7, 1995.

IMAGER FOR LOW ENERGY NEUTRAL ATOMS

P. Wurz, M.R. Aellig, P. Bochsler (Physikalisches Institut, University of Bern)

F. Herrero, M.F. Smith, D. Chornay, J. Keller (NASA, GSFC)

A. Ghelmetti, J. Quinn, E. Shelley, S. Fuselier (Lockheed Palo Alto Research Laboratory)

We describe a concept for an instrument to measure two-dimensional space plasma distributions by remote sensing of neutral atoms. The instrument measures one dimension, and from a spinning spacecraft one obtains two-dimensional line-of-sight maps of the neutral flux. Since we want to emply this instrument for measurements in the magnetosphere, the main species of interest are neutral H and O atoms with kinetic energies ranging from about 10 eV up to 1 keV. The instrument makes use of a low work function surface to convert neutral atoms efficiently to negative ions. The ions are accelerated away from the converter surface and brought to an intermediate focus by a large aperture lens. After further acceleration, the ions are deflected by a spherical electrostatic analyzer into a time-of-flight mass spectrometer. Mass resolution of the device is sufficient to resolve H, D, He, and O. Energy and azimuth angle information are obtained by positional imaging of the secondary electrons produced at the carbon foil. The large geometric factor combined with simultaneous angle-energy-mass measurements eliminates the need for cycling and provides the necessary high sensitivity for imaging at short time intervals. On a spinning spacecraft this instrument is capable of producing two-dimensional maps of low energy neutral atom fluxes.

(1) Chapman Conference on Measurement Techniques for Space Plasmas; April 3-7, 1995.

Neutral Atom Imaging Mass Spectrograph

P. Wurz, M.R. Aellig, P. Bochsler
Physikalisches Institut, University of Bern
Sidlerstrasse 5, 3012 Bern, Switzerland

A.G. Ghielmetti, E.G. Shelley, S. Fuselier
Lockheed Palo Alto Research Laboratory
3251 Hanover St., Palo Alto, CA 94304, U.S.A.

F. Herrero, M.F. Smith
Laboratory for Extraterrestrial Physics
NASA/GSFC Greenbelt, MD 20771, U.S.A.

T. Stephen
University of Denver
Denver, CO 80208, U.S.A.

submitted to

Optical Engineering
Special issue: "Swiss Imaging Instruments"

ABSTRACT

We describe a concept for an instrument to measure two-dimensiónal space plasma distributions by remote sensing of neutral atoms. The instrument measures in one dimension, and from a spinning spacecraft one obtains two-dimensional (line-of-sight) maps of the neutral flux. Since we want to employ this instrument for measurements in the magnetosphere, the main species of interest are neutral H and O atoms with kinetic energies ranging from about 10 eV up to 1 keV. The instrument makes use of a low work function surface to convert neutral atoms efficiently to negative ions. The ions are then accelerated away from the surface and brought to an intermediate focus by a large aperture lens. After further acceleration, the ions are deflected by a spherical electrostatic analyzer into a time-of-flight mass spectrometer. Mass resolution of the device is sufficient to resolve H, D, He, and O. Energy and azimuth angle information are obtained by position imaging of the secondary electrons produced at the carbon foil. The large geometric factor combined with simultaneous angle-energy-mass measurement eliminates the need for cycling and provides the necessary high sensitivity for imaging at short time intervals. On a spinning spacecraft this instrument is capable of producing two-dimensional maps of low energy neutral atom fluxes.

1. INTRODUCTION

One of the main objectives of space physics is to understand the Earth's magnetosphere and its interaction with the ionosphere and the energy input by solar radiation (photon and particle flux). These interactions are most readily observed in the high-latitude regions of the Earth's magnetosphere. The most widely known manifestation of these interactions are the auroral displays. After decades of *in situ* plasma measurements, which only provided point measurements at the location of the spacecraft, new instruments will have to provide maps of plasma distributions by remote sensing. The relevant length scales vary from > 10 km (auroral zone) to > 1 Earth radius (outer magnetospheric structure). In addition to the imaging capability, high temporal resolution — and thus high sensitivity — is necessary, since magnetospheric processes are of very transient nature. The time scales vary from minutes for the substorm onset to days for the decay of the ring current.

Fast neutral particles created from ions that undergo charge exchange upon collision with neutral gas atoms of the upper ionosphere and geocorona offer the potential for imaging the original charged particle distributions. These neutral particles are well suited for remote sensing since they are unaffected by the electro-magnetic fields and therefore follow ballistic trajectories. Neutral atom imaging is a relatively new technique [1] and several applications of this technique have been reported [2]. For energies larger than 10 keV, adaptations of standard instruments for measuring energetic ions can be used. A good review of the current status of this instrumentation is given by McEntire and Mitchell [1]. However, the energy range extending below about 1 keV contains a large fraction of the magnetospheric plasma and must be investigated to cover the full range of plasma energies in the magnetosphere. This energy range has been inaccessible to direct measurement so far. Significant improvements in detector and analyzer methods are necessary to make this energy range suitable for sensing the relatively low fluxes of neutral atoms.

Conventional techniques for measuring neutral particle fluxes rely either on direct detection via the energy deposition in solid state detectors, or on ionization and subsequent analysis in ion optical instruments. The former technique has been successfully applied for imaging energetic (>20 keV) atoms originating in the terrestrial ring current [3]. However, energy deposition in solid state detectors falls off rapidly below about 10 keV. The latter technique uses transmission ionization employing thin carbon-foils (C-foils) and provides reasonably high ionization yields (1 to 10%) in the energy range from about 10 to as low as 1 keV/nucleon [4,5,6]. For example, using ultra-thin C-foils in combination with highly sensitive analyzers, McComas et al. [7] have reported good efficiencies for negative O production at energies as low as 1 keV. However, at energies below this, the yield of secondary electrons decreases sharply [8].

Neither of the above conventional techniques are applicable for energies below 1 keV/nucleon. Since low energy neutral atom fluxes at all energies in planetary ionospheres and magnetospheres and in interplanetary space are generally many orders of magnitude lower than charged particle fluxes [1,2], a

highly efficient ionization process is required to convert these low fluxes into ic that can be subsequently detected. Combined with this high yield requirement are limitations on spacecraft resources (size, weight, and power). As a result, conventional laboratory ionization techniques for low energy neutrals are also not applicable. These techniques include electron ionization with its low overall yield and photon ionization with its impractical demands on spacecraft resources. Thus, until recently, imaging of very low energy (< 1 keV) neutral particles has remained impractical.

In the past 15 years new surface ionization techniques have been developed for applications in fusion plasma machines. With these techniques ionization efficiencies up to 67% in the energy range from several eV to about 1 keV [9,10,11] have been achieved. They make use of low work function surfaces for converting neutral particles to negative ions by resonant charge exchange after reflection from this converter surface. Surface ionization introduces new demands on design. These demands differ from conventional space flight instruments and require the development of new analyzer elements with matched ion optical properties.

In the following we describe a concept for an instrument capable of imaging low energy neutral H and O and to a lesser degree He atoms, the major species of interest for a magnetospheric application. Such an instrument would be suitable for imaging neutral atom fluxes from such diverse source regions as the cleft ion fountain and the interstellar neutral wind. Alternate concepts that combine surface conversion ionization techniques with a sp ograph have been described by Herrero and Smith [12] and by Gruntman [13].

2. REMOTE SENSING

A neutral atom imager in the magnetosphere detects neutral atoms created from charge exchange of plasma ions with the cold neutral background gas. Upon charge exchange, neutral atoms are no longer confined by the electric and magnetic fields in a plasma, and therefore follow ballistic trajectories. By recording the direction of the arriving particle, its energy, and its mass, the line-of-sight distribution of density, energy, and mass of the plasma volume can be deduced. This remote imaging technique has been applied for energetic neutral atoms in the Earth's ring current [3].

In the following we consider the case of imaging the cusp/cleft ion fountain and estimate the expected particle flux. Investigation of the cusp/cleft ion fountain is the original scientific goal behind the development of this instrument [14]. In this case, the low energy ions are ionospheric H^+ and O^+ flowing up along magnetic field lines at high latitudes in the auroral zone. These ions charge exchange with neutral H in the Earth's geocorona. The geometry of the remote sensing is shown in figure 1. Because the up-flowing ions in the cusp/cleft ion fountain gyrate around the magnetic field, we must cor er this special geometry in computing the neutral flux.

The probability for neutralization by charge exchange with the neutral background gas is given by

$$p(r) = 1 - e^{-\rho(r)\sigma l} \approx \rho(r)\sigma l \qquad \text{eq. 1}$$

with ρ the density of the background gas, σ the cross section for charge exchange, and l the path length. The latter approximation is easily justified by the low density of the background gas. The stream of emerging particles per second and unit area which have undergone charge exchange is then

$$J_{em} = j_{II}\, p(r) \qquad \text{eq. 2}$$

with j_{II} the current density of the up-flowing ions. The differential path length of the ions spiraling upwards is

$$dl = \left(1 + \left(2\pi f_c \frac{r_c}{v_{II}}\right)^2\right)^{\frac{1}{2}} dh \qquad \text{eq. 3}$$

with r_c the cyclotron radius, f_c the cyclotron frequency and v_{II} the velocity parallel to the magnetic field line. Thus we obtain

$$dJ_{em} = j_{II}\, \rho(r)\, \sigma \left(1 + \tan^2 \varphi\right)^{\frac{1}{2}} dh \qquad \text{eq. 4}$$

where

$$\tan \varphi = \frac{v_\perp}{v_{II}} = \frac{2\pi f_c r_c}{v_{II}}$$

and φ is the pitch angle given by the dipole approximation for the magnetic field

$$B = B_0 \left(\frac{R_0}{R}\right)^3$$

where R_0 is the location of the perpendicular acceleration of the ion. The energization occurs in a narrow, less than 100 km tall, altitude range to approximately the same energy [15]. B_0 is the magnetic field at R_0 and R is the location of the source volume (that is where the neutralization occurs). The gradient B force results in a change of φ

$$\sin \varphi = \sin \varphi_0 \left(\frac{R_0}{R}\right)^{\frac{3}{2}}$$

Having perpendicular acceleration at R_0 [15] we can set $\varphi_0 = 90°$ and finally obtain

$$\sin \varphi = \left(\frac{R_0}{R}\right)^{\frac{3}{2}} \qquad \text{eq. 5}$$

The number of neutral particles arriving at the location of the observer is given by the integral over the source volume

$$N_{arr} = c_\perp c_{II} \int_{width} \int_{height} \int_{depth} dN_{em} \qquad \text{eq. 6}$$

$c_\perp$ and c_{II} give the fraction of particles emitted in the direction of the observer (factors for direction perpendicular and parallel to magnetic field line), which are

$$c_\perp = \frac{a}{2\pi D} \text{ and } c_{//} = \frac{b}{\Delta\phi\, D}$$

where D is the distance from the plasma volume to the observer, $\Delta\phi$ is the width of the pitch angle distribution, and $a \times b$ is the size of the entrance aperture of the instrument. The number of particles entering the instrument is given by

$$N_{obs} = \int_{\omega_\perp} \int_{\omega_{//}} \int_{depth} N_{arr}\, dV_{source} \qquad \text{eq. 7}$$

with $\omega_\perp$ and $\omega_{//}$ the angles of acceptance of the instrument for a pixel. The width of the source volume is $\omega_\perp \cdot D$, the height of the source volume is $\omega_{//} D$, and the depth of the source volume is δ . Thus, the integral evaluates to

$$N_{obs} = j_{//}\, \rho\sigma \frac{1}{\cos\varphi} \underbrace{\left(\frac{ab}{2\pi\Delta\phi\, D^2}\right)}_{c_\perp c_{//}} \underbrace{(\omega_\perp \omega_{//} \delta D^2)}_{\substack{sampled \\ volume}} \qquad \text{eq. 8}$$

with the assumption that the source volume is uniform over the field of view. Equation 8 simplifies to

$$N_{obs} = \frac{j_{//}\, \rho\sigma}{2\pi\Delta\phi} \frac{A}{\cos\varphi} (\omega_\perp \omega_{//} \delta) \qquad \text{eq. 9}$$

with $A = a \times b$ the size of the entrance aperture of the instrument, which defines the pixel size.

For this estimate let us assume that the ion acceleration takes place at an altitude of 1000 km (R_0=7.4·10^6 m) and the source volume is located at an altitude of 2000 km (R=8.4·10^6 m). At these altitudes the only neutral species present in significant quantities is neutral hydrogen; at lower altitudes oxygen also has to be considered. The cross sections for the relevant charge exchange processes are $\sigma(H^+ + H \rightarrow H + H^+) \approx 4 \cdot 10^{-15}$ cm^2 [16] and $\sigma(O^+ + H \rightarrow O + H^+) \approx 1.2 \cdot 10^{-15}$ cm^2 [17]. There, the hydrogen density is $\rho \approx 10^4$ cm^{-3} [18]. However, the densities of neutral hydrogen and oxygen are a strong function of solar and geomagnetic activity. The current densities of the up-flowing ions at an ion energy of 100 eV are $j_{//}(O) \approx j_{//}(H) \approx 10^8$ ions/cm^2/sec [19]. The width of the pitch angle distribution is assumed to be $\Delta\phi = 30°$. With an instrument having a field of view of $\omega_\perp$=5° and $\omega_{//}$=5° and an entrance aperture of 1 cm^2, we obtain the expected fluxes from equation 8 as $N_{obs}(H) \approx 60$ atoms/sec/pixel and $N_{obs}(O) \approx 15$ atoms/sec/pixel. The estimated fluxes of neutral particles entering the instrument are rather small, but with efficient ionization of the incoming particles and the simultaneous measurement of mass, energy, and azimuth angle, mapping of the cusp/cleft ion fountain region is feasible, as will be shown below. A more elaborate estimate for the expected particle fluxes using a two-dimensional simulation has been given by Hesse et al. [20].

3. INSTRUMENT DESCRIPTION

3.1 Overview

The neutral atom imaging mass spectrograph discussed here combines state-of-the-art laboratory technology with flight-proven space plasma analyzer technology. A schematic cross section of the instrument in a plane containing the axis of symmetry is shown in Fig. 2. The principal elements of the instrument are an entrance collimating system, a conversion unit, an extraction lens, an electrostatic analyzer, and a carbon-foil TOF mass spectrometer with position sensing. Neutral and charged particles enter the sensor via the external aperture B1 and are collimated in angle and area by the entrance slit S1. An electrostatic deflector removes all incoming ions with energies less than 100 keV, while a broom magnet deflects all electrons with energies below 200 keV. The remaining neutral particles proceed until they strike the conversion surface (C) at a shallow angle, where a considerable fraction of the reflected particles becomes negatively charged. These negative ions are accelerated away from the converter surface and focused by a wide aperture low aberration lens (L) in the S2 slit plane. The conical slit, S2, is set to transmit ions with initial energies within a passband of about 10 eV < E < 1 keV. The transmitted ions are further accelerated to about 25 keV before they enter the electrostatic analyzer (EA), which is configured to be focusing in elevation angle in the image plane of the carbon foil. Upon striking the carbon foil, placed in the focal plane of the EA, the negative ions produce secondary electrons which provide the start pulse as well as the azimuth and radial position information. Particles (ions and neutrals) transmitted through the C-foil proceed to the stop MCP.

The entire instrument is rotationally symmetric about a vertical axis co-located with the S1 entrance slit. Particles that enter the analyzer through the slit S1 maintain their initial velocity direction except for non-specular reflection at the conversion surface. This effect is minimized through special ion optical design of the acceleration lens system and careful selection of the converter surface. As a result a direct correlation between the azimuth direction and the position on the plane of the carbon foil is achieved, which allows us to deduce the original velocity direction of the neutral atom. In a similar manner energy information is extracted from the radial impact position.

3.2 Collimator

All particles enter the instrument through aperture B1 and pass through a baffle system that prevents forward scattering of photons and particles through the use of serrated and blackened (CuS) surfaces. A pair of horizontal deflection plates sweep out charged particles with energies per charge less than 100 keV/e from the converter surface; a small broom magnet deflects electrons with energies below 200 keV. The required deflection plate voltages are about 5 kV. The collimator is fan-shaped to provide the desired wide azimuth acceptance, while the elevation angle acceptance is defined by the

heights of the B1 and S1 slits and their distance. A gas-tight shutter located behind S1 can be closed on command to protect the converter surface during launch and during the perigee portion of a low Earth orbit.

3.3 Conversion

As stated above, a low work function surface will be used to ionize the incoming neutral atoms. Surface ionization produces mainly single-charged negative ions, and works well for atoms with a positive electron affinity, like H and O atoms, which both have high electron affinities (0.75 eV and 1.46 eV). Particularly low work functions are obtained with monocrystalline tungsten W(110) substrates coated with a thin layer (0.6 monolayer) of cesium [21]. The Cs/W(110) combination takes advantage of the reduced work function due to the Cs overlayer on the metal (WF ≈ 1.45 eV), which gives high ionization rates. Under ideal laboratory conditions negative ion yields of up to 67% have been achieved [10]. Although most of the measurements have been done for H and D ionization due to their importance for fusion reactors, there are experimental results available also for O [22] and for He [23].

In order to select a converter surface which is best suited for space applications we carried out detailed computer simulations of the reflection and ionization of atoms from surfaces [24]. In addition to a high ionization efficiency, the angular scattering should be low, the ratio of energies of the reflected to the incoming particle should be close to unity, the particle reflection should be high, easy preparation of the surface in space, and low degradation with time are desired features. The particulars of the reflection of atoms from the converter surface were calculated with the MARLOWE computer program [25]. For the ionization efficiency, experimental and theoretical data were used [9, 10, 26, 27]. Several systems for the converter surface were investigated: Cs/W(110) with 0.6 and 1 monolayers of Cs, Ba(110), polycrystalline Ba, and Ba/Ag(111) with two monolayers of Ba.

Single crystal surfaces are much superior to polycrystalline or amorphous surfaces. The results of the computer simulations are summarized in Fig. 3 for the two most promising candidates so far, a Cs/W(110) surface with one monolayer of Cs and a Ba/Ag(111) surface. These two systems exhibit good reflection properties for particles and energy. Generally, small angular width of the reflected particle beam is only obtained for closed surfaces, especially if the filling of the crystal surface is high. This favors crystals with short atomic distances and closed-packed surfaces. The Cs/W(110) surface with 0.6 monolayers of Cs is not closed and therefore cannot be used for our application, although the energy reflection and the particle reflection efficiency are favorable in this system.

To achieve near specular reflection and high conversion efficiencies it is best to orient the target relative to the neutral beam at near grazing incidence. An impact angle of ≈ 75° from the surface normal appears to be the best choice to fulfill the above-mentioned criteria and ion optical constraints. This angle is somewhat shallower than in the original design of the instrument [28]. This change results from using single crystal surfaces instead of amorphous surfaces for particle reflection.

The theoretical results for the total conversion efficiencies for the converter surfaces are shown in Fig. 4 for the ionization of hydrogen atoms. For Cs/W(110) with one monolayer the total conversion efficiency rises from 5% up to 18% in the energy range from 10 eV to 300 eV for an angle of 75°. For the Ba/Ag(111) system the total conversion efficiency rises from 0.3% to 10% under the same conditions.

The conversion efficiencies, reflection properties (particles and energy), and the handling of these surfaces are currently investigated in a test stand in our laboratory [24]. Figure 5 shows the measured ionization efficiency of hydrogen molecules at a particle energy of 225 eV impinging on the Cs/W(110) surface under 80° with approximately one monolayer of Cs. Good ionization efficiencies are obtained, starting with an efficiency of 14% a few minutes after surface preparation. Our value for the efficiency agrees well with measurments reported by Amersfoort et al. [29]. For the same experimental setup they found ionization efficiencies around 10% for hydrogen atoms. Since the additional electron is bound stronger in the hydrogen molecule than in the hydrogen atom ($\approx$ 1.7 eV [30] and 0.75 eV, respectively) the higher ionization efficiency we find is no surprise. More important is however, that the conversion surface stayed functional during an entire day (24 h) of operations although the background pressure in our vacuum chamber was rather high (10^{-7} mbar). Also, the close correlation between work function of the converter surface and the ionization efficiency is clearly demonstrated in Fig. 5.

In the actual instrument the conversion unit consists of individual azimuthal facets, each aligned on a conical surface centered about the axis of rotational symmetry. The width of each facet is primarily driven by the azimuth angle resolution requirements. Nine facets, each spanning 10° in azimuth, were considered. The converter unit includes a cesium or barium dispenser (D) and a heater for baking the surface to remove undesired adsorbate contaminations. This allows for reconditioning the converter surface during flight when needed. To verify the condition of the surface it is necessary to measure its work function, since this is the determining parameter for the conversion efficiency (see figure 5). This is accomplished by illuminating the segments with light from three laser diodes at different wavelengths. The photo current resulting from emitted electrons from the converter surface is recorded and provides a good measure for the conversion efficiency (see Fig. 5), since the photon and negative ion production rates are both governed by the work function of the surface. During this operation the entrance slit shutter is closed to prevent interference by external UV light.

The required regeneration frequency will depend on the rate of deterioration of the surface. Special care must be taken to prevent contamination of the converter surface at launch and from low altitude exospheric gases. Generally, if the gas load to the converter surface is kept to less than one monolayer (10^{15} atoms cm^{-2}), the effects on conversion efficiency are expected to be small. For example, at an altitude of ~ 1 Re the expected average ram flux of hydrogen, the dominant constituent, is < 10^{8} atoms/cm^2/sec. Since more than 100 days are required for a monolayer of H

to form (assuming perfect sticking), this gas source will not pose a problem for the converter surface. Due to the much better vacuum in orbit than in our test stand, we estimate that regeneration of the converter surface will not be necessary more frequently than every 10 days for the proposed HI-LITE mission [14]. The entrance slit shutter will be closed during launch and during the low altitude portion of the satellite orbit to protect the conversion surface.

3.4 Extraction Optics

After acquiring a charge the negative ions are accelerated away from the surface by a wide aperture lens system (L). The potential distribution of the lens (Fig. 6) was designed to efficiently collect the ions produced on the converter surface and to focus them in the plane of the S2 slit. Equipotential surfaces are parabolically shaped over much of the interior region to minimize spherical aberrations. Figure 7 illustrates the achromatic focusing properties of the acceleration lens; specularly reflected ions are focused toward larger radii with increasing energy. Angle scattering about the specular reflection direction at the converter tends to broaden the focal spot. Since this effect is smaller than the energy dispersion, it is possible to extract moderate energy information from the radial position.

To minimize the effects of non-specular reflection on azimuth resolution (out of plane of Fig. 2) it is necessary to apply a high extraction field near the surface and to have a high ratio of final to initial energy. A lens extraction voltage of about 8 kV represents a good compromise between the requirements for energy dispersion and azimuth angle resolution. With this voltage, the beam spread in the azimuthal direction is sufficiently small to allow for ~ 5° azimuth resolution.

3.5 Electrostatic analyzer

The spherical electrostatic analyzer (EA) transmits all ions that passed through the collimating slit S2 to the TOF mass spectrometer because the range of initial energies is within the energy passband of the EA. It is geometrically configured to image the object slit S2 onto the C-foil. Thus the energy and azimuth angle information are conserved. Since the magnification of the EA is close to unity (-1), the more energetic ions are mapped to smaller radii. These elevation angle focusing and radial dispersion properties are illustrated in Fig. 8. In addition, the analyzer further provides for the desired UV-light filtering by introducing multiple surface reflections and solid angle attenuation.

3.6 Time-Of-Flight Mass Spectrometer

After deflection by the EA, the ions enter the mass spectrometer through the C-foil. The mass analyzer is a time-of-flight device using the C-foil technique [31]. The principal components of the TOF mass analyzer are the C-foil, field-free drift path for the ion and neutral particles, secondary electron extraction optics, and two multi-channelplate detectors (MCP1 and MCP2). Secondary electrons produced on the back side of the C-foils are

accelerated and focused onto MCP1, producing the start pulse for the TOF and providing position information. The signal produced at MCP2 by the primary particle provides the stop pulse for the TOF measurement. The azimuthal position can be derived from either MCP1 or MCP2. Both the start and stop signals are obtained from low (50%) transmission grids placed behind the respective MCP's. The anode behind the MCP1 grid is divided into 5 radial segments providing moderate energy resolution. Similarly, the anode behind the MCP2 grid is divided into 9 sectors providing 10° azimuth angle resolution. The position and TOF electronics are contained within the high voltage bubble. The encoded information is transmitted across the HV interface via fiber optics.

The time resolution of a C-foil TOF mass spectrometer is given as the sum of several factors which limit the accuracy of the time measurement

$$\left(\frac{\Delta T}{T}\right)^2 = \left(\frac{\Delta T_e}{T}\right)^2 + \left(\frac{1}{2}\frac{\Delta E_{foil}}{E}\right)^2 + \left(\frac{1}{2}\frac{\Delta E_{Range}}{E}\right)^2 + \left(\frac{\Delta L}{L}\right)^2 \qquad \text{eq. 10}$$

with T the total flight time of a particle, E the kinetic energy of the particle (25 keV in our case), and L the length of the field-free drift path of TOF (4 cm). ΔT_e is the resolution of the time measuring system, ΔE_{foil} is the energy straggling of the ion in the foil, ΔE_{Range} is the energy range of the primary particles, and ΔL is the variability of the flight path due to angular scattering in the carbon foil. The resolution of the time measuring system ΔT_e is given by the electronics and the time of flight dispersion of the start electrons and stop electrons, and amounts to 0.5 nsec. Therefore, ΔT_e is independent of the ion energy and the relative error $\Delta T_e/T$ is proportional to the velocity of the particle, i.e., to the square root of the energy

$$\frac{\Delta T_e}{T} = \frac{\Delta T_e}{L}\sqrt{\frac{2E}{M}} \qquad \text{eq. 11}$$

The energy straggling ΔE_{foil} is the width of the energy distribution of the ions at the exit of the carbon foil. According to Echenique et al. [32] and Beiersdorf et al. [33], the energy straggling is given by

$$\frac{\Delta E_{foil}}{E} \propto \frac{1}{\sqrt{M \cdot E}} \qquad \text{eq. 12}$$

The uncertainty of the kinetic energy of the ions when entering the TOF, $\Delta E_{Range}/E$, is given by the energy range of the primary particles, and also must be taken into account when evaluating the resolution of the entire TOF system. For our energy range from 10 eV up to 1 keV, $\Delta E_{Range}/E$ is at most ±2%. The angular scattering, $\Psi_{1/2}$, of particles passing the carbon foil causes a varying length of the flight path. According to Blokland [34], the half-width of the distribution of angles is

$$\Psi_{1/2} = 12.0 \cdot 10^3 \left(Z_1^{3/4} S / E\right) \qquad \text{eq. 13}$$

where Z_1 is the atomic number of the projectile, S is the area density of the carbon foil in $\mu g/cm^2$ and E is the kinetic energy in eV. Hence the variation of the length of the flight path is

$$\frac{\Delta L}{L} = \left(1 - \frac{1}{\cos(\Psi_{1/2})}\right) \qquad \text{eq. 14}$$

This contribution is small; the angular scattering is only important for small particle energies. Given that all ions have the same kinetic energy, the mass resolution is obtained from the time resolution by

$$\frac{M}{\Delta M} = \frac{1}{2}\frac{T}{\Delta T} \qquad \text{eq. 15}$$

In Table 1, mass resolutions are given for the particles of interest for an energy of 25 keV. Since this instrument is primarily sensitive to atoms with positive electron affinities, the TOF mass analyzer needs only to be able to separate H, D, He, and O in single charge state, which is easily achieved by this mass spectrometer. The requirements for mass resolution are rather modest compared with proven designs presently under development for space flight [35]. A simulated mass spectrum for typical abundances expected at 1000 km altitude is shown in Fig. 9. This simulation was done for a C-foil of 2 $\mu g/cm^2$ thickness.

4. DISCUSSION

Early space flight instruments performed differential measurements of ion distributions and required scanning in multidimensional parameter space for obtaining distribution functions. While most newer instruments are imaging spectrographs [7,35,36], they still rely on scans for covering the energy range. In the present instrument design we have carried the development one step further by measuring azimuth angle, energy, and mass simultaneously. This triple spectrographic imaging eliminates the need for a duty cycle, thus increasing sensitivity by the ratio of accumulation time per cycle step to the entire cycle time. Compared to conventional scanning analyzers (16 energy steps) our design provides approximately 20 times higher sensitivity. The absence of fast scanning of high voltages (HV) adds the benefit of simplified and lighter HV supply design.

The rotational symmetry of this design makes it possible to obtain a wide field-of-view in azimuth direction coupled with simultaneous imaging of the azimuth angle. Although the azimuth acceptance of the present optics is geometrically limited to ≈160° due to the flat field-of-view, such an instrument would nevertheless be able to cover more than 90% of the full 4π solid angle from a spinning spacecraft. Using a conical entrance field-of-view would permit coverage twice per spin. For source regions of spatially limited extent, such as the auroral acceleration region, a 2π instantaneous field-of-view provides no further benefits in geometric factor. The azimuth resolution that can be achieved with this type of instrument is intrinsically limited by the width of the entrance slit S1, the radius of the conversion surface, and the magnitude of the lens extraction voltage. For a 1 cm^2 entrance slit area and a 10 cm radius of the circle of converter surfaces, an angular resolution of ~5° is anticipated.

The ability to detect very low fluxes of neutral atoms relies on a low background from all sources. Although the TOF coincidence technique used here is inherently less sensitive to background, the large fluxes of EUV photons from the sun, geocorona and the Earth's limb would cause a serious background problem if not adequately suppressed. In the proposed design, the required attenuation is achieved by a combination of efficient light traps [12], multiple and diffuse surface reflections, and low reflectivity "black" surface coatings [37] at critical places. Besides the photon background, the two other major potential sources of background are photoelectrons from the converter surface and negative ions produced by dissociative attachment of photoelectrons to residual gas molecules. Due to the low work function of the converter surface, photoelectrons will be produced in large quantities. These electrons would produce unacceptably high chance coincidence rates if allowed to reach the TOF system, even though individually they could be discriminated due to their short flight times. To divert and trap these electrons a weak magnetic field is applied between the pole faces of M1 and M2 (Fig. 2). The ion background is minimized by maintaining a low residual gas pressure inside the instrument. A low outgassing rate of all internal surfaces coupled with a high conduction pumping port to outer space insures that a low internal pressure is maintained throughout the operational phase of the orbit. Furthermore, by quickly accelerating the photoelectrons away from the sensitive region, the probability for electron attachment is further reduced because the cross section for this process is inversely proportional to the kinetic energy. Negative ions produced by electron attachment from the residual gas proceed along somewhat different trajectories and are for the most part eliminated by the slit S2.

Sputtered (negative) ions, originating from energetic ion bombardment on the converter surface, also represent a potential source of background. Of primary concern are adsorbed gases on the surface, since W, Ba or Cs ions have very low transmission efficiencies in the TOF section and can easily be recognized by their large mass. Since energetic ions are abundant in Earth's orbit it is essential to reduce their fluxes. In the present design, ions with energies up to 100 keV/e are rejected by an electrostatic deflector in the entrance collimating system.

A critical element of the instrument is the neutral to ion conversion technique. The experience from our test stands shows that it is possible to maintain the converter surface in reasonably good shape for a day. In the good vacuum in space this translates to at least ten days or more of continuous operation before reconditioning becomes necessary. After reconditioning the surface for an estimated 10 to 100 times during a mission, the average contamination with Cs on internal surfaces of the sensor, other than on the converter itself, is expected to be less than one monolayer. Since the vapor pressure of a Cs monolayer is very low, migration of Cs between different parts of the instrument is minimal. Nevertheless, special design precautions are taken to guard all internal high voltage insulators (e.g., individual guard baffles). No deterioration of the MCP detectors, which are well shielded behind the carbon foils, is expected at the estimated Cs evaporation levels.

While cesiate conversion surfaces have been thoroughly investigated in the laboratory environment, they have, to our knowledge, thus far not been applied to space instrumentation. It is the goal of our ongoing research effort to develop this novel technology for use on spacecraft instrumentation.

5. CONCLUSIONS

We have developed a concept for a new type of mass spectrograph that is specifically designed to provide two-dimensional images from ion distributions by remote sensing of the emitted neutral particles on space platforms. The instrument summary is given in Table 2. The instrument covers the energy range from about 10 to 1000 eV, and the mass range from 1 to 20 amu with mass resolution sufficient to separate all the masses of interest H, D, He, and O. Its large geometric factor (0.14 cm^2sr) for a 90° field-of-view combined with high conversion, transmission, and detection efficiencies and a 100% duty cycle, result in the high sensitivity necessary for imaging the low energy outflow from the high latitude ionospheric acceleration regions. Using the fluxes given in section 2 or by Hesse et al. [20] we estimate count rates from the ion fountain source region of ~ 1 to 10 Hz per 10° azimuth pixel for the HI-LITE orbit, thus providing a reasonably well defined image within 5 minutes.

6. ACKNOWLEDGMENTS

This research was supported by the Swiss National Science Foundation and by Lockheed Independent Research.

6. REFERENCES

1. R.W. McEntire and D.G. Mitchell, *Instrumentation for global magnetospheric imaging via energetic neutral atoms*, Geophysical Monograph 54, *Solar System Plasma Physics*, edts. J.H. Waite Jr., J.L. Burch, and R.L. Moore (1989), 69-80.

2. K.C. Hsieh, C.C. Curtis, C.Y. Fan, and M.A. Gruntman, *Techniques for remote sensing of space plasma in the heliosphere via energetic neutral atoms: A review*, in Remote Sensing of Plasmas, 357, (1992), 357-364.

3. E.C. Roelof, *Energetic neutral atom image of a storm-time ring current*, Geophys. Res. Lett., 14, (1987), 652.

4. M. Gonin, A. Bürgi, M. Oetliker, and P. Bochsler, *Interaction of solar wind ions with thin carbon foils - Calibration of time-of-flight spectrometers*, ESA SP-348, (1992), 381.

5. A. Bürgi, M. Oetliker, P. Bochsler, J. Geiss, M.A. Coplan, *Charge Exchange of Low-Energy Ions in Thin Carbon Foils*, J. Appl. Phys. 68 (1990) 2547-2554.

6. R. Kallenbach, M. Gonin, A. Bürgi, and P. Bochsler, *Charge Exchange of Hydrogen Ions in Carbon Foils*, Nucl. Instr. Meth. (1993) in press.

7. D.J. McComas, B.L. Barraclough, R.C. Elphic, H.O. Funsten III, and M.F. Thomsen, *Magnetospheric imaging with low-energy neutral atoms*, Proc. Natl. Acad. Sci., 88, (1991), 9598.

8. H. Grünwaldt, K. Gringauz, I. Axford, C. Becker, H. Dinse, F. Gliem, P. Király, I. Klimenkov, A. Remizou, A. Richter, W. Rieck, W. Riedler, H. Rosenbauer, R. Schmidt, K. Schwingenschuh, M. Steller, Szalai, K. Szegö, G. Vladimirova, M. Verigin and B. Wilken, Proceedings of the IVth International Seminar on Manufacturing of Scientific Space Instrumentation, Academy of Sciences of the USSR, Space Research Institute, (1989) 7-27.

9. J.N.M. Van Wunnik, J.J.C. Geerlings, E.H.A. Granneman, and J. Los, *The scattering of hydrogen atoms from a cesiated tungsten surface*, Surf. Sci. 131, (1983), 17.

10. J.J.C. Geerlings, P.W. van Amersfoort, L.F.Tz. Kwakman, E.H.A. Granneman, J. Los, *H^- formation in proton-metal collisions*, Surf. Sci. 157, (1985), 151.

11. J. Los and J.J.C. Geerlings, *Charge exchange in atom surface collisions*, Phys. Reports 190, (1990), 133.

12. A. Herrero, *Light trap cavity design using multiple reflections and solid angle attenuation: Applications to a spaceborne electron spectrometer*, Applied Optics Vol 31, (1992), 5331.

13. M.A. Gruntman, *In situ measurements of the composition (H, D and O atoms) of interstellar gas*, Report Np. 102 M, University of California L.A., U.S.A. (1991).

14. M.F. Smith, F. Herrero, M. Hesse, D.N. Baker, P. Bochsler, P. Wurz, H. Balsiger, S. Chakrabarti, G. Erikson, D. Cotton, T. Stephen, C. Jamar, J.C. Gerard, S.A. Fuselier, A.G. Ghielmetti, S.B. Mende, W.K. Peterson, E.G. Shelley, R.R. Vondrak, D. Gallagher, T.E. Moore, C. Pollock, R. Arnoldy, M. Lockwood, R. Gladstone, *The High-Latitude Ion Transport and Energetics Explorer (HI-LITE): A Mission to Investigate Ion Outflow from the High-Latitude Ionosphere*, SPIE proceedings, 2008 (1993), 40-56.

15. B.A. Whalen, S. Watanabe, and A.W. Yau, *Observations in the transverse ion energization region*, Geophys. Res. Lett. 18, (1991), 725-728.

16. R.A. Mapleton, *Theory of charge exchange*, Wiley-Interscience, New York, (1972), 209-240.

17. W.L. Fite, A.C.H. Smith, and R.F. Stebbings, *Charge transfer in collisions involving symmetric and asymmetric resonances*, Proc. Roy. Soc. London A268 (1962) 527.

18. D.J. McComas, B.L. Barraclough, R.C. Elphic, H.D. Funsten III, M.F. Thompson, *Magnetospheric imaging with low-energy neutral atoms*, Proc. Natl. Acad. Sci. 88 (1991), 9598.

19. A.W. Yau, E.G. Shelley, W.K. Peterson, and L. Lenchyshyn, *Energetic auroral and polar ion outflow at DE 1 altitudes: Magnitude, composition, magnetic activity dependence, and long-term variations*, J. Geophys. Res. 90 (1985), 8417-8432.

20. M. Hesse, M.F. Smith, F.A. Herrero, A.G. Ghielmetti, E.G. Shelley, P. Wurz, P. Bochsler, D. Gallagher, T.E. Moore, T. Stephen, *Imaging ion outflow in the high-latitude magnetosphere using low-energy neutral atoms*, SPIE Proceedings Vol. 2008, (1992), 83-92.

21. J.L. Desplat and C.A. Papageorgopoulos, *Interaction of cesium and oxygen on W(110) I. Cesium adsorption on oxygenated and oxidized W(110)*, Surf. Sci. 92, (1980), 97.

22. H.M. van Pinxteren, C.F.A. van Os, R.M.A. Heeren, R. Rodnik, J.J.C. Geerlings, and J. Los, *Angular Selection Rules for the Resonant Population of $O^-(^2P)$ and $C^-(^4S)$ in Grazing Ion-Surface Collisions*, Europhys. Lett. 10 (1989) 715-719.

23. H. Verbeek, W. Eckstein, and P.J. Schneider, *The negative Fraction of Deuterium and Helium Scattered from a Sodium Surface*, Proceedings of the Third International Symposium on Production and Neutralization of Negative Ion Beams, American Institute of Physics (1984) 273

24. M.R. Aellig, Master Thesis, University of Bern, (1994), Bern, Switzerland.

25. M.T. Robinson, *Slowing-down time of energetic atoms in solids*, Phys. Rev. B40 (1989), 10717-10726.

26. C.F.A. van Os, P.W. Amersfoort, and J. Los, *Negative ion formation at a barium surface exposed to an intense positive-hygrogen ion beam*, J. Appl. Phys. 64 (1988), 3863-3873.

27. U. van Slooten, O.M.N.D. Teodoro, A.W. Kleyn, J. Los, D. Teillet-Billy, and J.P. Gauyacq, *Negative ion formation in proton scattering from Ba/Ag(111)*, Chem. Phys. 179 (1994), 227-240.

28. P. Wurz, P. Bochsler, A.G. Ghielmetti, E.G. Shelley, F. Herrero, and M.F. Smith, *Concept for the Hi-Lite neutral atom imaging instrument*, Proceedings of the Symposium on Surface Science, edt.: P. Varga and G. Betz, Austria, (1993), 225-230.; P. Wurz, P. Bochsler, A.G. Ghielmetti, E.G. Shelley, F. Herrero, and M.F. Smith, *Remote Imaging of Ion Distributions Using Low Energy Neutral Atoms*, Helv. Phys. Acta 66, (1993), 445-446.; A.G. Ghielmetti, E.G. Shelley, S. Fuselier, P. Wurz, P. Bochsler, F. Herrero, M.F. Smith, T. Stephen, *Mass Spectrograph for Imaging Low Energy Neutral Atoms*, Opt. Eng. 33, (1994), 362-370.

29. P.W. van Amersfoort, J.J.C. Geerlings, L.F.Tz. Kwakman, A. Hershcovitch, E.H.A. Granneman, and J. Los, *Formation of negative ions on a cesiated W(11) surface; the influence of hydrogen implantation*, J. Appl. Phys. 58 (1985) 3566-3572.

30. T.E. Sharp, *Potential energy diadram for molecular hzdrogen and its ions*, Lockheed Palo Alto Research Laboratory, LMSC 5-10-69-9 (1969) 1-84.

31. G. Gloeckler, and K.C. Hsieh, *Time-Of-Flight Technique for Particle Identification at Energies from 2-400keV/Nucleon*, Nucl. Instr. Meth. 165, (1979), 537-544.

32 P.M. Echenique, R.M. Nieminen, J.C. Ashley, and R.H. Ritchie, *Nonlinear stopping power of an electron gas for slow ions*, Phys. Rev. A 33, (1986) 897-904.

33. P. Beiersdorf, A.L. Roquemore, and R. Kaita, *Characteristics of Compact Solid-Target Charge Exchange Analyzers for Energetic Ion Diagnostics on Tokamaks.* Rev. Sci. Instrum., 58 (1987) 2092-2098.

34. A.A.E.v. Blokland, T.W.M. Grimbergen, and H.W.v.d. Ven, *A mass selective neutral particle energy analyzer with background rejection.* Rev. Sci. Instrum., 63(3), (1992) 1978-1987.

35. H. Rème, J.M. Bosqued, J.A. Sauvaud, A. Cros, J. Dandouras, C. Aoustin, Ch. Martz, J.L. Médale, J. Rouzaud, E. Möbius, K. Crocker, M. Granoff, L.M. Kistler, D. Hovestadt, B. Klecker, G. Paschmnn, M. Ertl, E. Künneth, C.W. Carlson, D.W. Curtis, R.P. Lin, J.P. McFadden, J. Croyle, V. Formisano, M. Di Lellis, R. Bruno, M.B. Bavasanno-Cattaneo, B. Baldetti, G. Chionchio, E.G. Shelley, A.G. Ghielmetti, W. Lennartsson, A. Korth, H. Rosenbauer, I. Szemerey, R. Lundin, S. Olsen, G.K. Parks, M. McCarthy, and H. Balsiger, *The ion spectrometry experiment to measure the properties of the ionic plasma composition and distribution function at energies between ~0 and 40 keV/e*, in "The Cluster Mission", ESA SP-1103, (1988), 65.

36. G. Shelley, A.G. Ghielmetti, H. Balsiger, R.K. Black, J.A Bowles, R.P. Bowmann, O. Bratschi, J.L. Burch, C.W. Carlson, A.J. Coker, J.F. Drake, J. Fischer, J. Geiss, A. Johnstone, D.L. Kloza, O.W. Lennartsson, A.L. Magoncelli, G. Paschmann, W.K. Peterson, H. Rosenbauer, T.C. Sanders, M. Steinacher, D.M. Walton, B.A. Whalen, and D.T. Young, *The toroidal imaging mass-angle spectrograph (TIMAS) for the polar mission*, Space Sci. Rev. (1994), submitted.

37. H. Balsiger, P. Eberhardt, J. Geiss, A. Ghielmetti, H.P. Walker, and D.T. Young, *A satellite-borne ion mass spectrometer for the energy range 0 to 16 keV*, Space Sci. Instr. 2, (1976), 499.

Figure Captions:

Figure 1. Schematics of HI-LITE mission. The spacecraft will be placed in an elliptical orbit of 250 km by 4500 km at an inclination of 65°. 10 sectors will be used for angular mapping, the rotation of the satellite for lateral mapping of the plasma volume.

Figure 2. Schematic drawing of the instrument with the principal components. The entrance collimating system defines the elevation angle acceptance through slits B1 and S1 and contains the ion and electron deflectors I-DEF and E-DEF. Other key elements are the conversion surface C, the cesium dispenser D, the secondary electron guiding magnets M1 and M2, extraction lens L, energy limiting slit S2, spherical electrostatic analyzer EA, and the time-of-flight mass analyzer MA.

Figure 3. Results of the MARLOWE computer simulation for H atoms reflected from a Cs/W(110) surface with one monolayer of Cs, and from a Ba/Ag(111) surface with two monolayers of Ba. The individual curves are calculations for 65° (solid line), 70° (dashed line), 75° (pointed line) and 80° (dashed-pointed line). The curves in the upper right panel are calculations for 100 eV (dashed line) and 300 eV (solid line).

Figure 4. Results of the MARLOWE computer simulation for the total conversion efficiencies versus kinetic energy for H atoms reflected from Cs/W(110) surface and Ba/Ag(111) surface. The individual curves are calculations for 65° (solid line), 70° (dashed line), 75° (pointed line) and 80° (dashed-pointed line).

Figure 5. Measured ionization efficiency of H_2 at 225 eV impinging on Cs/W(110) under 80° with approximately one monolayer of Cs (solid line). The work function is measured with photo effect (dashed line). The degradation of the ionization efficiency with time is due to the moderate pressure (10^{-7} mbar) in the vacuum chamber.

Figure 6. Equipotential lines in extraction lens between converter surface C and exit slit S2.

Figure 7. Trajectories of ions originating at the converter surface with energies of 10 eV and 100 eV respectively. Reflection angles are ± 10° from the specular direction (65°). Total acceleration potential up to S2 is 8 keV.

Figure 8. Ray-tracing of ions in the spherical electrostatic analyzer originating at the object slit S2 with angle and energy dispersion defined by the extraction lens. Geometric parameters are center radius 62 mm, sector angle 155°, plate separation 24 mm.

Figure 9. Simulated mass spectrum for the TOF mass analyzer using ion abundance occurring at an altitude of 1000 km. The ion abundance and the mass resolution used for this simulation are given in Table 1.

Table 1: Mass resolution of the time-of-flight mass spectrometer at an ion energy of 25 keV for a C-foil thickness of approximately 2 $\mu g/cm^2$. Also the values for the approximate ion abundance at an altitude of 1000 km are given.

species	abundance [relative to H]	energy per nucleon [keV/nuc]	$\Delta\tau/\tau$	$m/\Delta m$
^1H	1	25	0.0279	17.9
^2D	$1.8\ 10^{-4}$	12.5	0.0282	17.7
^3He	$5\ 10^{-5}$	8.33	0.0281	17.8
^4He	0.1	6.25	0.0277	18.1
^{16}O	1	1.56	0.0281	17.8

Table 2: Summary of instrument characteristics.

Energy Range:	10 eV to ~ 1000 eV
Energy Resolution:	~ 5 steps
Mass Range:	H, D, He, O (in principle unlimited)
Field-of-View:	
Azimuth:	90°
Elevation:	8°
Angle Resolution:	
Azimuth:	10°
Elevation:	10°
Detection efficiency:	
Conversion Efficiency:	see figure 5
Mass Analyzer Efficiency:	0.4
Geometric Factor:	0.14 cm^2sr

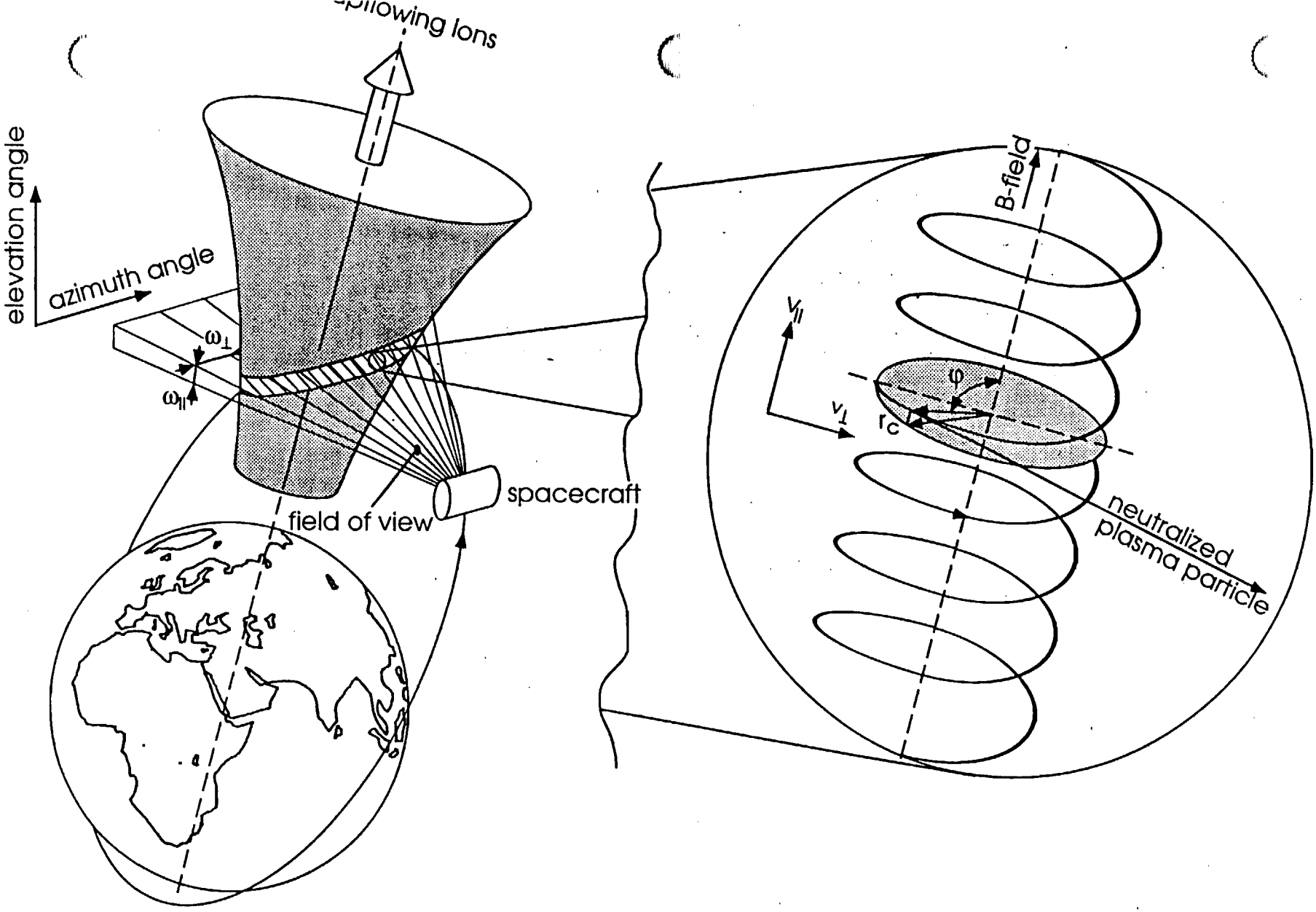
upflowing Ions
elevation angle
azimuth angle
$\omega_\perp$
$\omega_\parallel$
field of view
spacecraft
B-field
$v_\parallel$
$v_\perp$
r_c
φ
neutralized
plasma particle

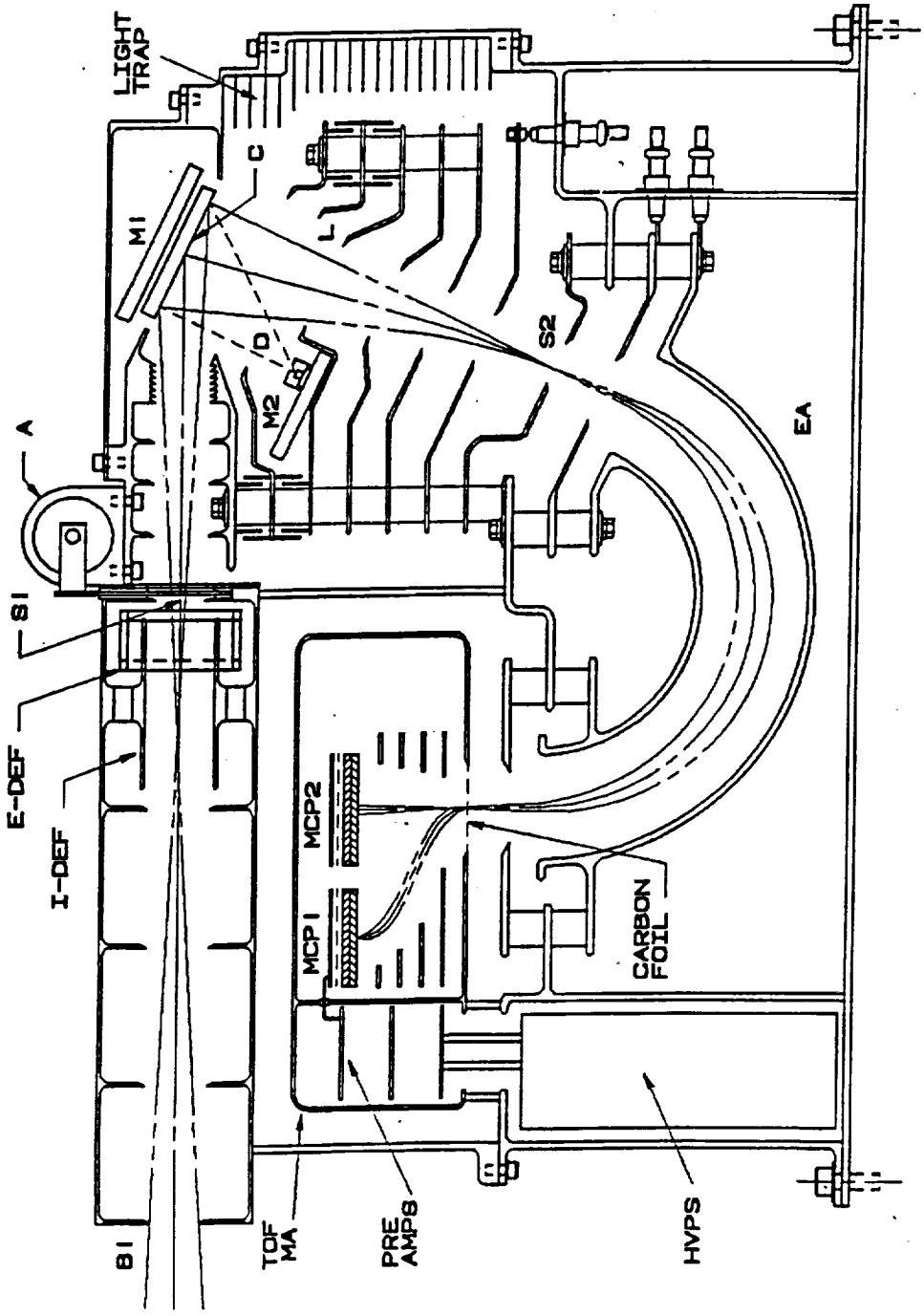
LIGHT TRAP
C
M1
L
S2
D
M2
A
EA
S1
E-DEF
I-DEF
MCP2
MCP1
CARBON FOIL
B1
TOF MA
PRE AMPS
HVPS

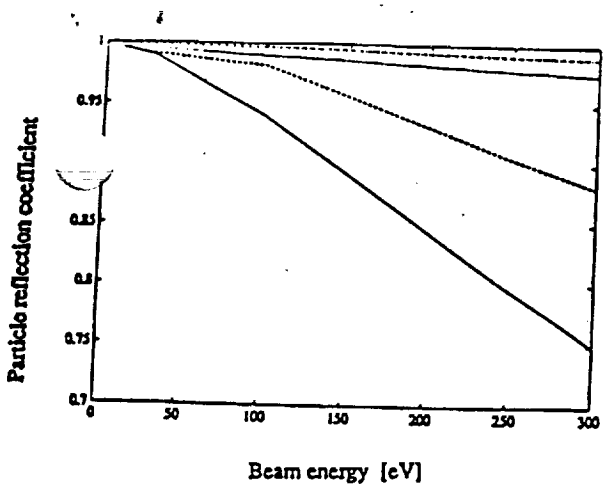
Particle reflection coefficient
Beam energy [eV]

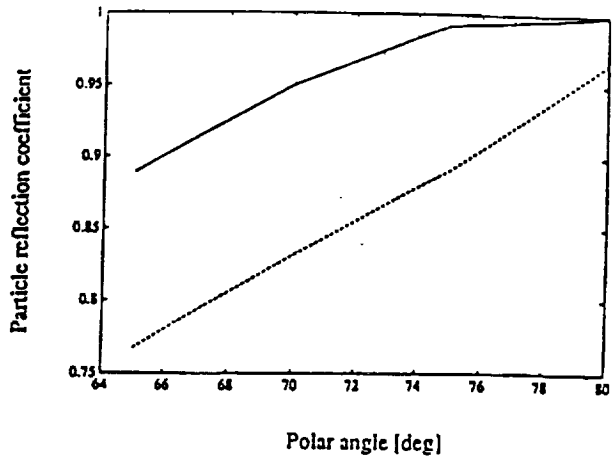
Particle reflection coefficient
Polar angle [deg]

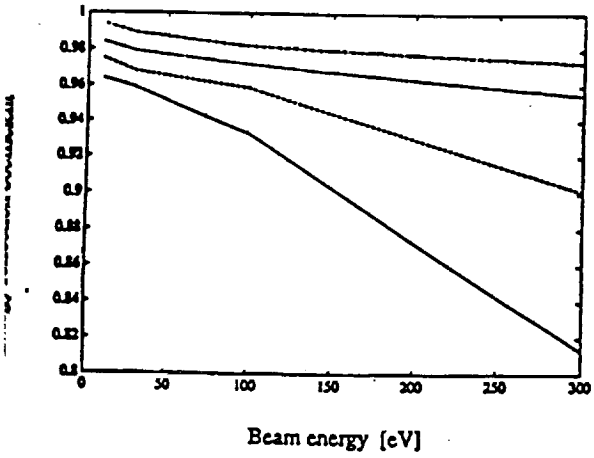
Beam energy [eV]

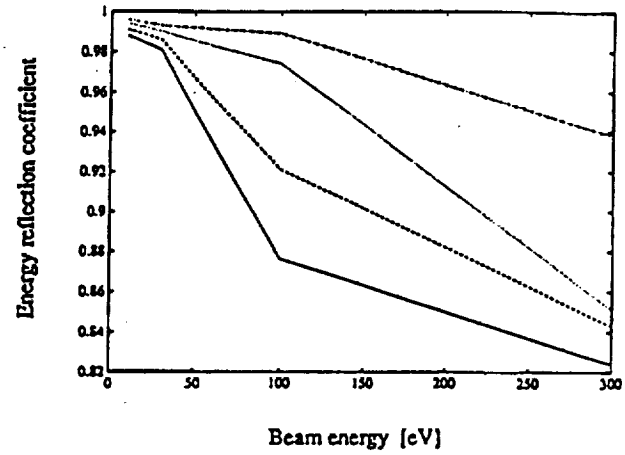
Energy reflection coefficient
Beam energy [eV]

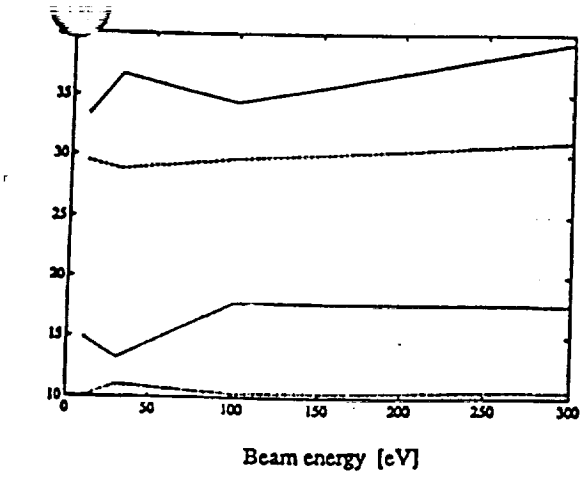
Beam energy [eV]

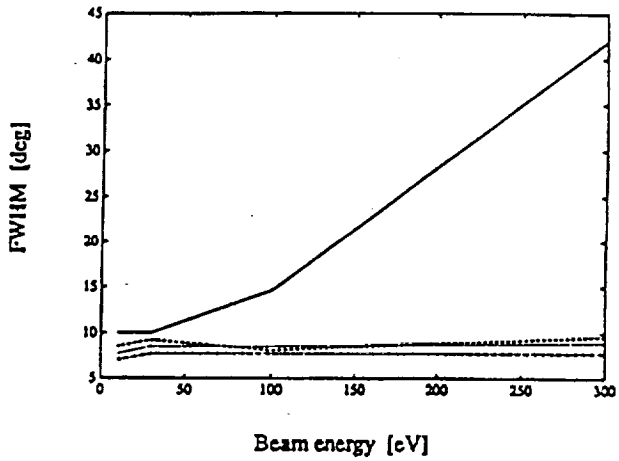
FWHM [deg]
Beam energy [eV]

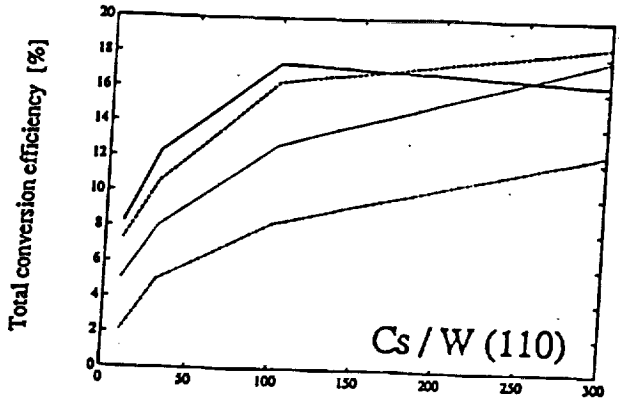
Total conversion efficiency [%]
Cs / W (110)
Beam energy [eV]

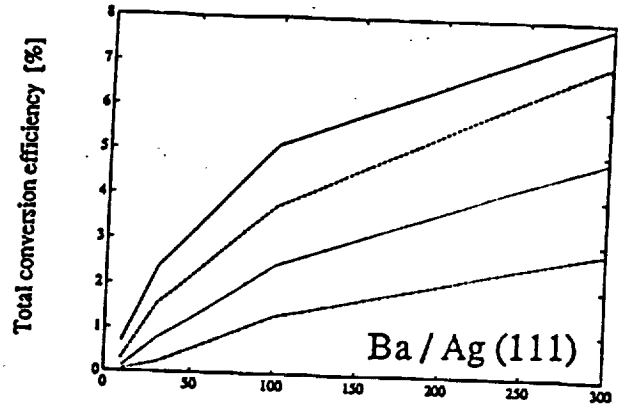
Total conversion efficiency [%]
Ba / Ag (111)
Beam energy [eV]

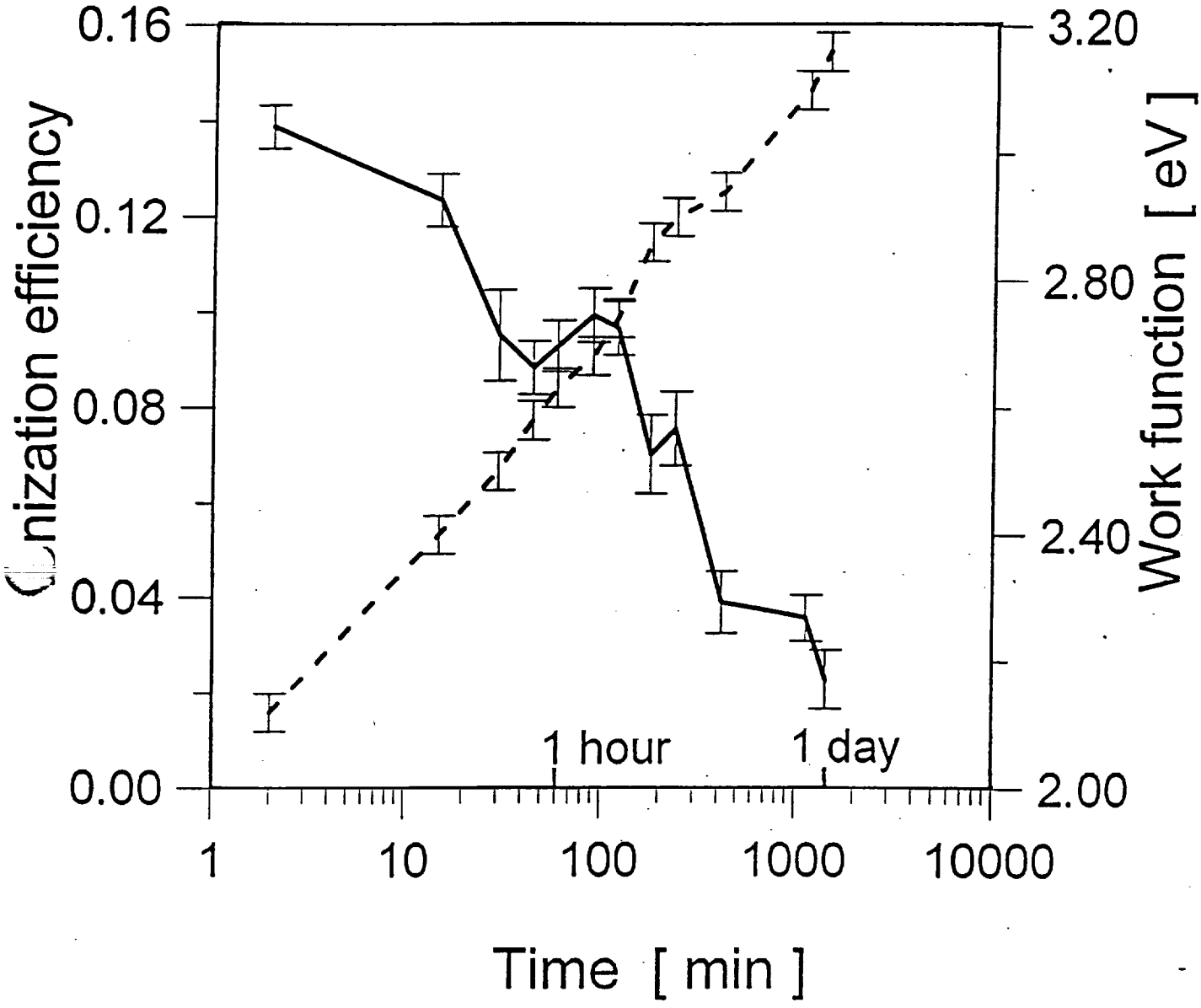
0.16
0.12
0.08
0.04
0.00
nization efficiency
3.20
2.80
2.40
2.00
Work function [eV]
1 hour
1 day
1
10
100
1000
10000
Time [min]

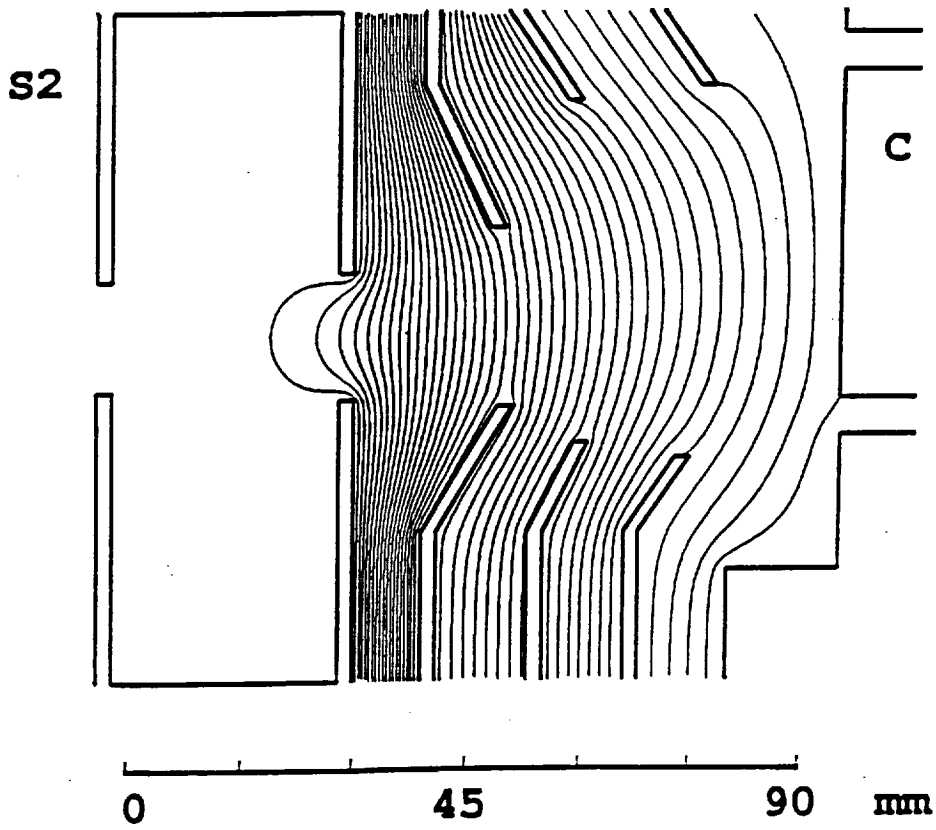
S2
C
0
45
90
mm

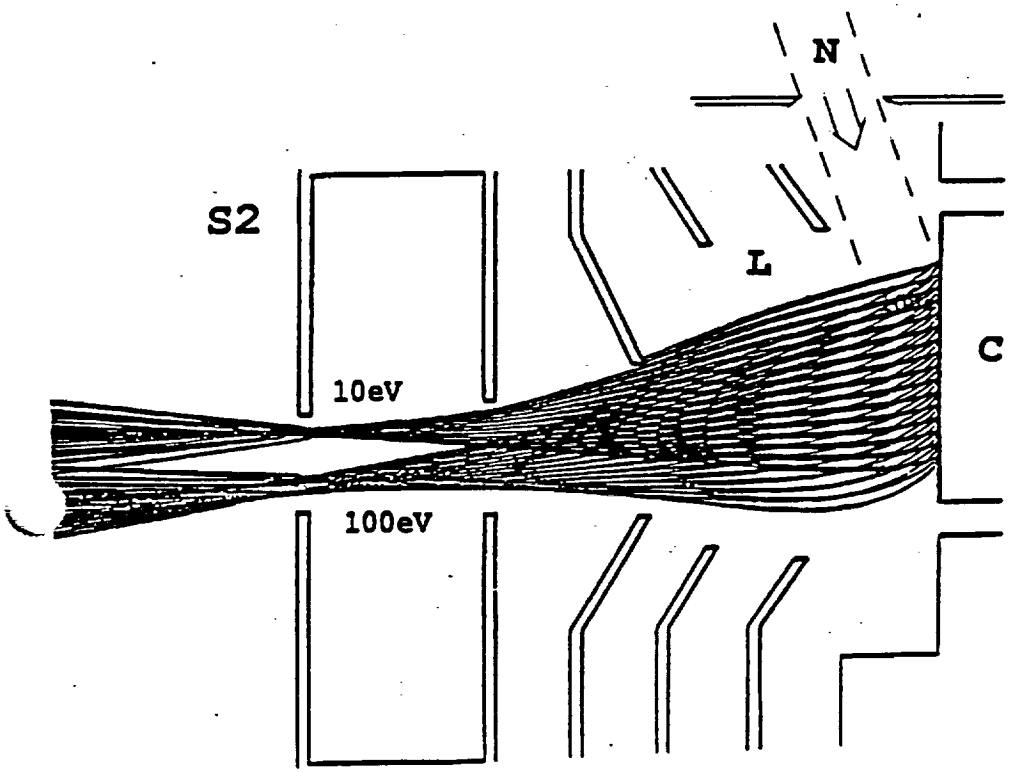
N
S2
L
C
10eV
100eV

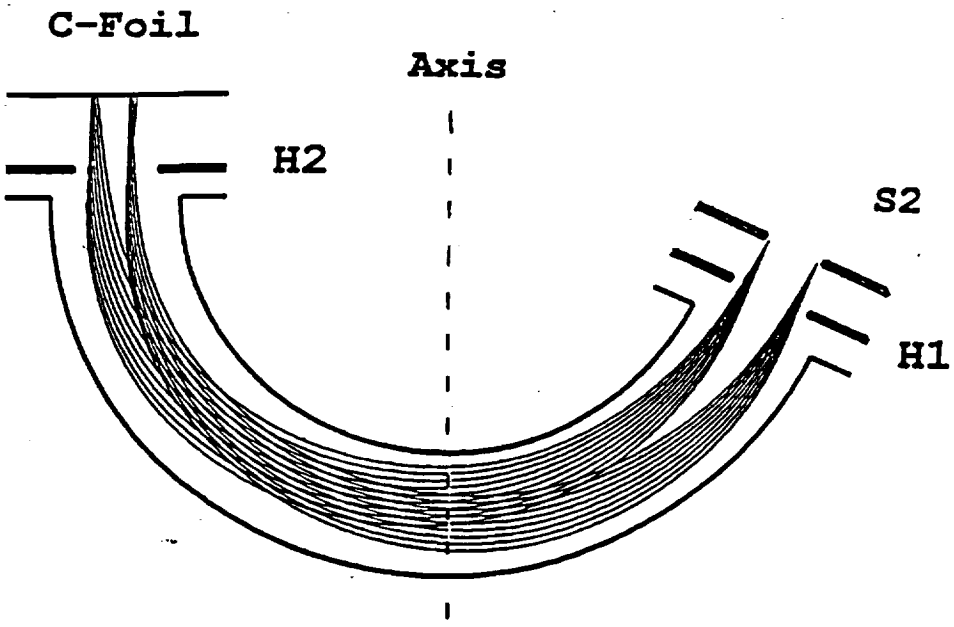
C-Foil
Axis
H2
S2
H1

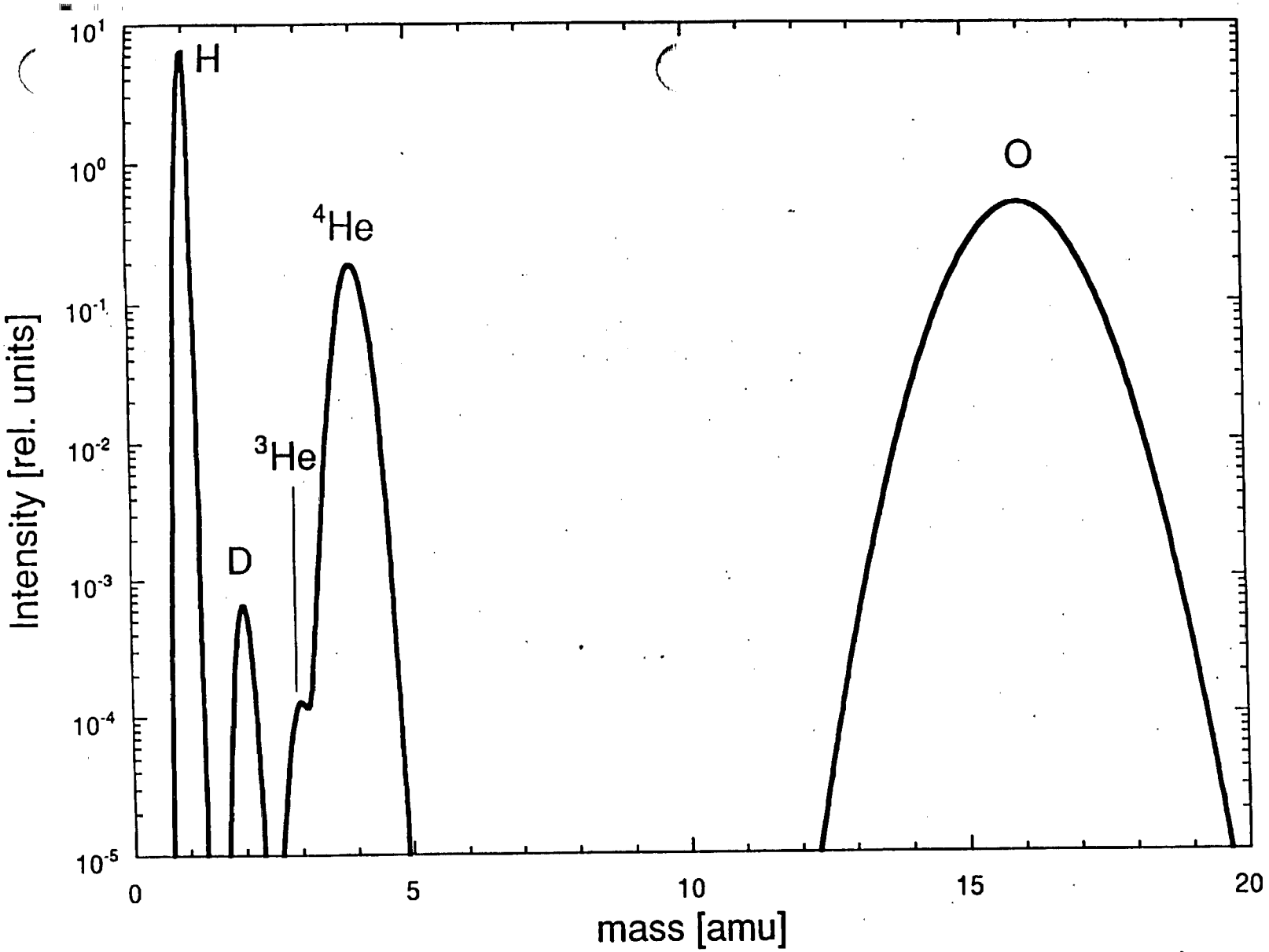
H
D
^{3}He
^{4}He
O
Intensity [rel. units]
mass [amu]
10^1
10^0
10^{-1}
10^{-2}
10^{-3}
10^{-4}
10^{-5}
0
5
10
15
20